Materials Today Bio 24 (2024) 100898

Contents lists available at ScienceDirect

Materials Today Bio

journal homepage: www.journals.elsevier.com/materials-today-bio

A novel on-a-chip system with a 3D-bioinspired gut mucus suitable to investigate bacterial endotoxins dynamics

L. Sardelli [a], M. Campanile [a], L. Boeri [a], F. Donnaloja [a], F. Fanizza [a], S. Perottoni [a], P. Petrini [a], D. Albani [b], C. Giordano [a,*]

[a] Department of Chemistry, Materials and Chemical Engineering 'Giulio Natta,' Politecnico di Milano, Milan, Italy
[b] Department of Neuroscience, Istituto di Ricerche Farmacologiche Mario Negri IRCCS, Milan, Italy

ARTICLE INFO

Keywords:
Dynamic culture
Microenvironment
Microfluidic devices
Lipopolysaccharide
Gut-brain-axis
Microbiota

ABSTRACT

The possible pathogenic impact of pro-inflammatory molecules produced by the gut microbiota is one of the hypotheses considered at the basis of the biomolecular dialogue governing the microbiota-gut-brain axis. Among these molecules, lipopolysaccharides (LPS) produced by Gram-negative gut microbiota strains may have a potential key role due to their toxic effects in both the gut and the brain.

In this work, we engineered a new dynamic fluidic system, the MINERVA device (MI-device), with the potential to advance the current knowledge of the biological mechanisms regulating the microbiota-gut molecular crosstalk. The MI-device supported the growth of bacteria that are part of the intestinal microbiota under dynamic conditions within a 3D moving mucus model, with features comparable to the physiological conditions (storage modulus of 80 ± 19 Pa, network mesh size of 41 ± 3 nm), without affecting their viability (~ 10^9 bacteria/mL). The integration of a fluidically optimized and user-friendly design with a bioinspired microenvironment enabled the sterile extraction and quantification of the LPS produced within the mucus by bacteria (from 423 ± 34 ng/mL to 1785 ± 91 ng/mL). Compatibility with commercially available Transwell-*like* inserts allows the user to precisely control the transport phenomena that occur between the two chambers by selecting the pore density of the insert membrane without changing the design of the system. The MI-device is able to provide the flow of sterile medium enriched with LPS directly produced by bacteria, opening up the possibility of studying the effects of bacteria-derived molecules on cells in depth, as well as the assessment and characterization of their effects in a physiological or pathological scenario.

1. Introduction

The interaction between the gut microbiota and human cells affects the health status of different regions of the body, even if they are anatomically distant from the gastrointestinal tract [1]. Increasing resources have been devoted to model the gut environment and to study the communication between bacteria and human cells to address various biological questions. One of the most exciting examples of bacteria-host interaction is the microbiota-gut-brain axis, a new paradigm for research [2–4]. The shift of the microbial population toward a pathological profile, defined as dysbiosis, may trigger chronic inflammation that influences the onset and progression of many diseases [5–16].

In the challenging track to understand and reproduce the microbiota-gut-brain axis, increasing resources have been devoted to study *in vitro* the relation between the gut microflora and the brain function under healthy and pathological conditions.

This challenge is addressed through various approaches, each capable of examining a different nuance within such a complex framework [17–20]. For instance, the co-culture of bacteria and cells facilitated the identification of the pathological effects of specific bacterial species (such as *E. coli* and *B. Fragilis*) or the probiotic effects of others (like *L. rhamnosus* GG) [21–23]. Complementarily, individual cultures of cells or bacteria have allowed a more in-depth exploration of the microbiota-gut dialogue at a molecular level, pinpointing molecules of bacterial origin that have become subjects of study due to their potential pathological effects [19,24]. Embracing the second approach, the ERC-CoG project 'MINERVA' aimed at developing an advanced technological platform for investigating the correlation between gut microflora and brain functionality within both healthy and pathological contexts [19,24].

* Corresponding author.
E-mail address: carmen.giordano@polimi.it (C. Giordano).

https://doi.org/10.1016/j.mtbio.2023.100898
Received 2 May 2023; Received in revised form 20 November 2023; Accepted 1 December 2023
Available online 10 December 2023

The full description of the biological mechanisms behind this communication is still an open challenge. Although several hypotheses have been proposed in the last decades [17,25] most of the studies have been focused on the immunomodulatory and potential toxic effects of bacterial-derived molecules released at both peripheral and central levels [26–38]. Among these, lipopolysaccharides (LPS) are particularly relevant. LPS are components of the outer membrane of Gram-negative bacteria that can target various cellular receptors such as toll-*like* receptor (TLR) 4 and myeloid differentiation protein 88 (MyD88), leading to a downstream molecular cascade that causes the activation of a variety of pro-inflammatory genes [39]. Pathological concentration and distribution of LPS were found in various individuals with different neurodegenerative diseases. For example, in patients with Alzheimer's disease (AD), the plasma concentration of LPS is three times higher than in healthy individuals (between 20 and 60 pg/mL) and LPS deposition was detected in the AD amyloid plaques [40,41].

Because of their importance in pathophysiology, LPS are used in different ways, either *in vivo* or *in vitro*, to study the communication between bacteria and host cells [42]. *In vivo*, LPS are typically injected directly into the point of interest or administered orally and then the presence of neuropathological biomarkers, behavioral changes, or the development of AD-related symptoms are monitored [43–45]. Similarly, LPS can also be used *in vitro* to treat intestinal, immune, and brain cell-based models cultured in standard multi-well plates to elucidate various aspects of the molecular mechanisms behind the toxicity of LPS [46–48].

In vivo, bacterial LPS do not directly reach the intestinal cells, but they must first cross the environment that separates the bacterial community from the gut cells [49–51]. This environment, that can be considered as the stage where the dialogue between bacteria and cells is performed, is the intestinal mucus.

The intestinal mucus is a biological hydrogel composed mainly of high molecular weight glycoproteins (*i.e.*, mucins) and has the function of providing the intestinal bacteria with an environment suitable for colonization while preventing infection of the epithelium [52,53]. This function is based on the viscoelastic properties that are specifically distributed throughout the thickness of the mucus layer. Toward the lumen, the mucus layer is loose and permeable to bacteria, allowing them to survive and be metabolically active in symbiosis with the human body. In contrast, the mucus layer proximal to the epithelium is compact and prevents bacterial penetration. Not only the different viscosity along the mucus layer has a role: the chemical moieties and the polymeric network affect diffusion with a combined and interdependent effect on viscosity. The different functions of the mucus layers are marked by a different mesh size, about 30–200 nm in the loose layer and 7–50 nm in the inner layer [54,55].

Various mucus models have been proposed in the literature, including physiological mucus models, mono-component mucus models and multi-component mucus models [56]. They are generally composed by mucin solutions, with or without gelling additives, and other mucus components such as albumin, lipids, and DNA. These models may be further added onto cell monolayers to improve their physiological similarity [57,58]. However, they have been mainly exploited in drug delivery studies [59–61], with only limited use in the investigation of the role of LPS in the bacteria-cell communication.

Different parameters of the *in vivo* situation, like the transepithelial electric resistance (TEER), physiologically similar villous structure, clearance and flushing of substances, can be reproduced with increased similarity by microfluidic devices, such as gut-on-a-chips, that may be comprehensive of mucus models [20,62]. In these dynamic systems, endotoxin activity can be monitored directly by injecting LPS into the media circuit or indirectly by culturing LPS-producing bacteria such as, *E. coli* and *B. fragilis*, to study the control mechanisms of gut barrier function, immune modulation, bacterial-cell interactions and inflammation [23,63].

However, gut-on-a-chip devices are specifically designed to study the biological effect of endotoxins, or the presence of bacteria, directly on cells. Mucus, whenever is considered, is used as a static component of the system, made by commercially available or cell-secreted mucin layers on membranes.

Although considered as an important component in the interaction between bacteria and cells, there are still gaps in the integration of microfluidic devices with *in vitro* mucus models that are bioinspired in terms of mechanical and microstructural properties [56,57]. In this view, a recent work proposed a mucus-on-a-chip device investigating the diffusion of mucoadhesive or muco-penetrant nanoparticles using a static mucus model prepared from solubilized mucins (1 % w/v) in PBS (*i.e.,* no 3D structure). Although not focusing on aspects like physiological motion, bioinspired properties and suitability for bacterial culture, this microfluidic system posed a significant advance in the field, as it addressed mucus as a stand-alone and cell-free toll to study intestinal transport phenomena [64].

We hypothesize that the synergy between a controlled dynamic stimulation and a bioinspired physiological-*like* mucus microenvironment will lead to advances in our understanding of the effect of bacterial molecules on human health. Hence, the final aim of this work is to engineer a dynamic fluidic tool, the MINERVA device (MI-device), bridging the gap between gut-on-a-chip devices and *in vitro* mucus models by assessing two main functions (Fig. 1). Firstly, the MI-device will support the culture of bacteria in an *ad hoc* compartment, specifically designed to host a 3D mucus model, named I-Bac3Gels, that is bioinspired in terms of properties relevant for the modelling of the gut barrier such as microstructure and viscoelastic properties. Secondly, the MI-device will allow the controlled production, diffusion and sterile extraction of LPS produced by the bacteria dynamically cultured in the mucus model at quantifiable concentrations.

As source of LPS, we selected two *E. coli* strains (ATCC 12014 and CCUG 11412) that have been associated to human pathological scenarios of both gut [65,66] and other organs including the brain [67,68] and whose LPS toxicity was already evaluated *in vitro* [69,70] and *in vivo* [71,72]. Moreover, they have been already cultured in microfluidic devices [73,74] as representative of LPS-producing bacteria [59,72,73].

2. Materials and methods

2.1. Materials

The intestinal mucus model was developed by crosslinking an alginate solution. Alginate powder (sigma Aldrich, Lot MKCJ8027), $CaCO_3$ (Caelo ph 9.0 Lot 18,057,507) and D-(+)-gluconic acid-delta-lactone (GDL) (Sigma-Aldrich G4760; Lot SLBM7762V) were used to produce the intestinal mucus model. Dulbecco's Modified Eagle Medium (DMEM) (EuroClone ECM0101L; Lot EU M035455) and Luria Bertani Broth (LB) (Formedium LMM0 102; Lot FMDA114005176), Agar (Formedium, Lot12/MFM/113) and sodium citrate (Sigma Aldrich, Lot BCBW9965) were used for bacterial study.

2.2. Optimization of the intestinal mucus model I-Bac3Gel

2.2.1. Engineering the I-Bac3Gel as physiological-like microenvironment

2.2.1.1. Production of the intestinal mucus model. The intestinal mucus models (I-Bac3Gels) were developed by crosslinking an alginate solution. Alginate was dissolved in complete DMEM (20 % FBS, 1 % L-glutamine) for at least 12 h and then mixed with $CaCO_3$ suspension, fresh complete DMEM medium and GDL solutions in a volume ratio of 4:1:1:1. The initial concentration of alginate, calcium salt and GDL were selected to reach, respectively, the final concentration of 1 % (w/v), 0.1 % (w/v) and 1 % (w/v).

2.2.1.2. Stability assessment. The I-Bac3Gels were prepared as described

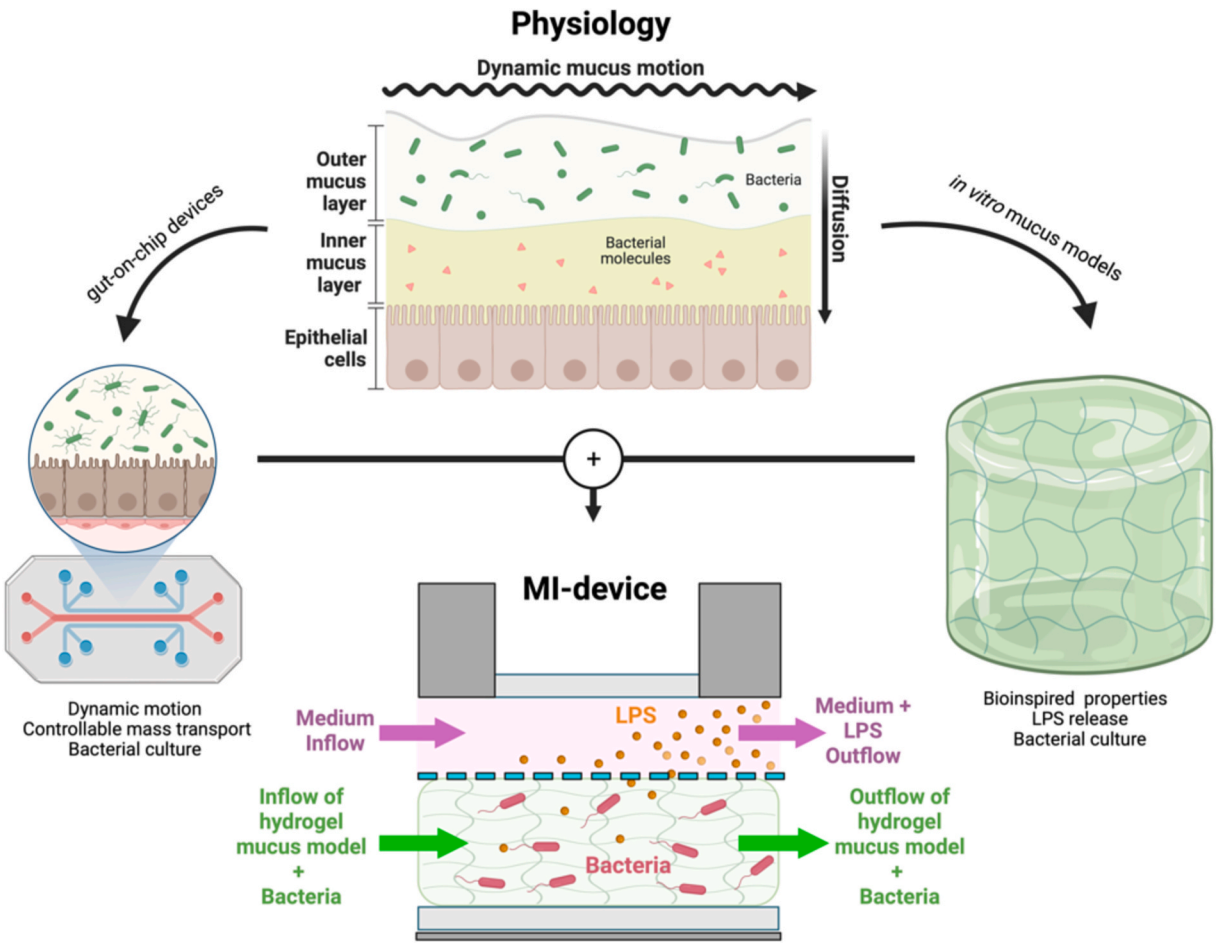

Fig. 1. Schematic representation of the MI-device rationale (bottom, centre): it has been designed to fill the gap between the classical gut-on-a-chip approach (left, representative picture of a gut-on-chip device) and the *in vitro* modelling of the intestinal mucus (right, representative image of a hydrogel). The dynamicity and high level of control over the mass-transport phenomena that are typical of fluidic devices are synergically coupled with the bio-similarity in terms of viscoelastic properties and microstructure of the optimized intestinal mucus model.

above. Immediately after production, 2 mL of the hydrogels were poured into PET transparent inserts compatible with 6-Transwell-*like* multwell-plates and stored in fridge (4 °C). After 24 h, the Transwell-*like* inserts with the completely crosslinked intestinal mucus model were weighted, 2 mL of fresh medium was poured into the basal chamber thus touching the PET membrane and the inserts incubated at 37 °C. After 1, 7, 14 and 21 days the stability was assessed by weighting the model and the weight normalized with reference to the initial one ($w(\%)$ at t_0 equals to 100 %). Stability was hence defined as described by the formula (equation (1)):

$$w(\%) = \left(1 + \frac{w(t) - w(t_0)}{w(t_0)}\right) \bullet 100 \tag{1}$$

2.2.1.3. Modelling the microbiota environment: rheological characterization of the intestinal mucus model. Immediately after production, 2 mL of hydrogels were poured into petri dishes (diameter 35 mm) and stored in fridge (4 °C) for 24 h. 1 h before analysis, the models were maintained at room temperature and then analysed. A rotational rheometer (Anton Paar, Modular Compact Rheometer MCR 502) with parallel plate geometry (diameter 25 mm) was used to apply an oscillatory shear strain of 0.5 % with variable frequency from 0.1 to 20 Hz at the temperature of 25 °C (gap between plates equal to 0.5 mm).

2.2.1.4. Estimation of the intestinal mucus model microstructure. The frequency responses were interpreted by using the Generalized Maxwell model (GMM) as previously reported [75,76]. Briefly, the GMM models the viscoelastic material as the parallel of n (viscoelastic) elements, each one made by a spring in series with dashpot, with viscoelastic moduli (G' and G'') described by equation (2) and equation (3).

$$G' = G_e + \sum_{i=1}^{n} G_i \frac{(\lambda_i \omega)^2}{1 + (\lambda_i \omega)^2}; G_i = \frac{\eta_i}{\lambda_i} \tag{2}$$

$$G'' = \sum_{i=1}^{n} G_i \frac{\lambda_i \omega}{1 + (\lambda_i \omega)^2}; G_i = \frac{\eta_i}{\lambda_i} \tag{3}$$

with $\lambda_{i+1} = 0.1 \bullet \lambda_i$

where λ_i and η_i are, respectively, the relaxation time and the viscosity of the i-esimal element, G_e the modulus of an elastic element in parallel to the other Maxwell elements and ω the angular velocity (*i.e.*, $\omega = 2\pi f$). By minimizing the error between GMM and the experimental data [77,78], it possible to define the optimal-fitting GMM and estimate the material shear modulus, G_∞, and mesh size, ξ (distance between two crosslinking sites on the same polymeric chain) as:

$$G_\infty = G_e + \sum_i^n G_i \tag{4}$$

$$\xi = \sqrt[3]{\frac{6RT}{\pi N_A G_\infty}} \tag{5}$$

where R is the universal gas constant, T the absolute temperature and N_A the Avogadro's number. In this work, the fitting of the rheological data

with the GMM models was performed using MATLAB.

2.2.1.5. Diffusivity of pathological lipopolysaccharides. The I-Bac3Gels were produced similarly as described above, using DMEM without FBS with the addiction of commercial LPS-FITC (Signa-Aldrich, Lot 000119070) as fluorescent probe for the diffusion analysis. Briefly, alginate solution, LPS-FITC-enriched DMEM, $CaCO_3$ suspension and GDL solution were mixed in volume a ratio of 4:1:1:1 to reach the final concentration, respectively, of 1 % (w/v), 100 μg/mL, 0.1 % (w/v) and 1 % (w/v). Then, 300 μL of the model enriched in LPS-FITC were poured into the wells of a 48-wells multiwell plate and stored in fridge for 24 h. At complete crosslinking, 300 μL of fresh medium were poured in direct contact with the intestinal mucus model and sampled (200 μL) at different time points, namely 15, 30 min after the addiction of the medium and then every hour for 5 h. The amount of LPS-FITC diffused from the hydrogel to the medium was quantified by measuring the fluorescence of the sample (wavelength of 488 nm).

2.2.2. Biological and functional validation of the intestinal mucus model

2.2.2.1. Inoculum of E. Coli. Two *E. coli* strains (ATCC 12014 serotype O55:K59(B5):H- and CCUG 11412 serotype O111:K (58):H-) were collected by scraping frozen aliquots with microbiological loop and inoculated overnight in 10 mL Luria-Bertami (LB) broth at 37 °C (shaking of 300 rpm). The resulted *E. coli* suspensions were diluted in complete DMEM (20 % FBS, 1 % L-glutamine) accordingly to the needs for the infection of the intestinal mucus model or suspended cultures (*i.e.*, planktonic controls).

2.2.2.2. E. coli static culture condition. The two *E. coli* strains were embedded separately in the intestinal mucus model by modifying the production process of the hydrogels. Alginate solution, *E. coli* suspension, $CaCO_3$ suspension and GDL solution were mixed in a volume ratio of 4:1:1:1 to reach the final concentration of 1 % (w/v), $5{\cdot}10^4$ bacteria/mL and 1 % (w/v), respectively. Then, 2 mL of the mucus model with embedded *E. coli* were poured into the wells of a 6-well multiwell plate. Then, transparent (pore density of $2{\cdot}10^6$ pores/cm^2) or translucent (pore density of $1{\cdot}10^8$ pores/cm^2) PET inserts compatible with the 6-well multiwell plate were placed onto the hydrogels and filled with 2 mL of fresh medium to provide nutrients to the bacteria. Finally, the models with embedded *E. coli* were incubated for 24, 48 and 72 h at 37 °C.

2.2.2.3. E. coli viability in the intestinal mucus model. The assessment of *E. coli* viability was performed by CFUs counting on LB-agar plates (2.5 % (w/v) LB culture medium containing 1.5 % (w/v) agar, Difco) [79]. At different time points (24, 48 and 72 h) the mucus model was dissolved by mixing the hydrogel with 3 mL of 50 mM sodium citrate solution. The samples with bacteria were then homogenized and serially diluted in PBS up to $1{:}10^{-8}$. Finally, 10 μL of the diluted bacteria suspensions were poured onto LB-agar plates and incubated at 37 °C overnight. The following day, CFUs were manually counted to estimate, thought the dilution factor, the bacterial concentration obtained in the different culture conditions.

2.2.2.4. Quantification of the lipopolysaccharide production in the intestinal mucus model. After 24, 48 and 72 h, the medium in the inserts was collected to investigate the presence of LPS by Limulus Amebocyte Lysate (LAL) test. The samples were firstly diluted to reach the sensitivity range of the reaction (0.01–0.1 ng/mL). Then, the LAL test was performed following the manufacturer guidelines: duplicates of 50 μL of medium were mixed with 50 μL of the reconstituted LAL reagent and 100 μL of the chromogenic substrate provided, while maintaining the temperature at 37 °C. The reaction was stopped after 6 min by adding 25 % (v/v) acetic acid and the absorbance (407 nm) measured by means of a spectrophotometer. Finally, the concentration of LPS (ng/mL) was obtained by comparing data with standard curves.

2.3. Engineering the MI-device

2.3.1. Design and development

The MI-device was designed to support the 3D dynamic culture of bacteria while allowing the secretome diffusion in sterile medium by exploiting a bicameral configuration. The device was developed to be assembled by a plug and play approach with commercially availabe 6-well multiwell Transwell-*like* inserts, thus maximizing a user-friendly configuration and comparability with standard culture set-up. Indeed, each device consists in an apical and a basal component that envelop the insert thus forming two hemi-chambers separated by a semipermeable PET membrane. The pore dimension and pore density of the membrane between the two hemi-chambers can be controlled by selecting the insert type in order to investigate the diffusion of target molecules in different conditions. In this work, two different membranes were used to study the mass transport of bacterial-derived LPS from the basal to the apical hemi-chamber in condition of higher pore density ($1{\cdot}10^8$ pores/cm^2, translucent inserts) and lower pore density ($2{\cdot}10^6$ pores/cm^2, transparent inserts) but with the same pore dimensions (diameter of 0.4 μm). Multi jet fusion 3D printing of Nylon PA12 was used to manufacture the different compartments of the device. The basal hemi-chamber was produced with an elliptical base (4 cm × 2 cm) to host the mucus model for 3D culture of bacteria. Its elliptical shape was designed in order to support the mucus flow and avoid stagnation points. The apical hemi-chamber was designed as a cylinder of diameter equal to 1 cm in order to fit the 6-well multiwell Transwell-*like* inserts for either parallel or antiparallel medium flow. The thickness was set to 2 mm for the both apical and basal hemi-chambers. Silicon tubes and luer-lock connectors allow the connection of the device to the perfusion systems and reservoirs for sample collection. Both the apical and basal hemi-chambers are equipped with a glass-slide to allow the possible real-time live monitoring of the culture.

2.3.2. Hydraulic sealing and sterility assessment

The hydraulic sealing was assessed by placing two plastic O-ring system bonds in both the hemi-chambers and a snap-fit closure. Different flow rates of distilled water (0.5, 1, 5, 10, 20, 50, 100, 200 and 400 μL/min) were imposed in both the hemi-chambers to investigate the presence of fluid leakage, The flow rate was maintained for at least 12 h before investigating possible fluid leakage. For the sterility assessment, the MI-devices were decontaminated using vaporized hydrogen peroxide (VHP LS60 Biodecontamination Unit, STERIS), while silicon tubing and reservoirs were autoclaved. Inflow of LB medium was set at 50 μL/min and maintained overnight. Then, 10 μL of the medium were collected from the reservoirs and from the two hemi-chambers, and poured onto LB-agar plate to investigate bacterial presence after 24 h.

2.4. Integrating the MI-device and the I-Bac3Gels

2.4.1. E. coli dynamic 3D culture in the MI-device

I-Bac3Gels with embedded *E. coli* were produced as described above. Immediately after preparation, 35 mL of infected mucus model were poured into luer-lock syringes and connected to the basal chamber of the MI-device by means of 20 cm silicon tubes (I.D. 1.58 mm). Similarly, syringes with 35 mL of sterile complete DMEM were connected to the apical chambers of the MI-device by 20 cm long silicone tubes (I.D. 1.58 mm). The basal and apical outlets were connected to sterile reservoirs for sample collections. The inlet syringes were placed into a multi-syringes syringe-pump (Harvard apparatus PHD ULTRA) and a constant flow rate of 5.0 μL/min was set to start the hydrogel and medium flows. After 24, 48 and 72 h of culture at 37 °C, the medium, from the apical chamber, and the infected hydrogels, from the basal chamber, were sampled for the quantification of LPS and bacterial availability investigation respectively. The dynamic cultures and the downstream

analysis were performed considering four different scenarios:

a) *E. coli* ATCC cultured in device mounted with transparent (T) insert;
b) *E. coli* ATCC cultured in device mounted with translucent (L) insert;
c) *E. coli* CCUG cultured in device mounted with transparent (T) insert;
d) *E. coli* CCUG cultured in device mounted with translucent (L) insert.

The infected hydrogel taken from the basal hemi-chamber was mixed in a volume ratio of 1:1.5 with 50 mM sodium citrate, homogenized and serially diluted following the same procedure of the static cultures (see Paragraph 2.2.2). Then, 10 μL of the diluted sample were poured onto LB agar plate and incubated at 37 °C overnight before manual counting of the CUFs.

2.4.2. Quantification of the lipopolysaccharide production in the MI-device

Before the quantification of LPS, the sterility of the medium collected from the apical hemi-chamber was verified by plating 10 μL onto LB-agar plates and incubated overnight at 37 °C. The samples were diluted to reach the sensitivity level of the LAL test (0.01–0.1 ng/mL). The quantification of LPS was obtained by following the manufacturer instruction as reported above (see Paragraph 2.2.2.4.)

2.5. Evaluation of the effect of the lipopolysaccharides produced in the MI-device on gut epithelial cells

2.5.1. Static culture of in vitro model of human intestinal epithelial cells

Caco-2 cells (ATCC® HTB-37) were cultured as 2D *in vitro* model of human intestinal epithelial cells. The culture medium used for the cell culture was high glucose DMEM supplemented with 20 % heat-inactivated FBS, 2 mM L-glutamine, 100 units/mL of penicillin and 100 μg/mL of streptomycin. Caco-2 cells were seeded at a density of $5{\cdot}10^4$ cells/cm^2 onto pH-equilibrated PET membrane of translucent (L) Transwell-*like* inserts having surface area of 1.1312 cm^2, pore diameter of 0.4 μm, and pore density of $1{\cdot}10^8$ pores/cm^2. The L-inserts with cells were placed in an incubator at 37 °C with 5 % CO_2 for 7 days, and the culture medium was replaced every 2 days.

2.5.2. Evaluation of the epithelial integrity

ATCC *E. coli* was cultured for 72 in 3D dynamic condition within the MI-device mounted with translucent (L) Transwell-*like* insert (see Paragraph 2.4.1). At the end of the culture, the DMEM culture medium in the reservoirs placed downstream of the apical hemi-chamber was collected and stored at −80 °C.

After 7 days of static culture (see Paragraph 2.5.1), the 2D monolayer of Caco-2 cells were treated with the medium collected from the apical chamber of the MI-device and the monolayer integrity evaluated by light microscopy (Leica DMi1 optical microscope) and by measuring the TEER as previously reported [48,80]. One electrode of the EVOM (World Precision Instruments, USA) measuring system was placed in the apical compartment of the Transwell-*like* insert (L), while the second one put in contact with the basal compartment. The TEER (Ω·cm^2) of the Caco-2 monolayer was estimated according to equation 6

$$TEER_{cells} = (R_{measured} - R_{blank}) \cdot \text{Membrane Area} \quad (6)$$

where the Membrane Area is equal to 1.1312 cm^2 and R_{blank} is the resistance (Ω) of the translucent (L) Transwell-*like* insert without cells. The values of TEER at different time points of treatment with LPS-enriched culture medium (3, 4, 7, 10, 11, 14, 17, 18 and 21 days) were obtained by averaging three measures per conditions. The experiment was conducted twice.

2.6. Statistical analysis

Unless stated, experiments were performed at least three times, each with at least duplicate samples, and data were plotted as mean ± standard deviation. Normality test (D'Agostino-Person test) was performed to investigate the Gaussian distribution of the data. Then, Student's t-test/Mann-Whitney test or ANOVA/Kruskal-Wallis test were performed to compare couple or group of data, accordingly to the normality check results.

3. Result

The rationale of the present work was to employ an engineering approach to meet the need of new systems addressing the relevance for human physiopathology of bacteria-derived biomolecules. In particular, we developed a technological tool to provide LPS that are directly produced by bacteria in a biosimilar microenvironment, in a quantifiable and controllable way. Firstly, we optimized a 3D *in vitro* intestinal mucus model, focusing on the key properties required to support bacterial culture and allow the transport and diffusion of LPS (see Paragraph 3.1). These properties included the stability, the viscoelasticity, and the size of the polymeric network mesh. We engineered a new dynamic device (see Paragraph 3.2), the MI-device, to provide a user-friendly system, featuring standard biology laboratory tools, such as the Transwell-*like* inserts, with the advantage of providing dynamic stimulations through both flowing liquid culture media and moving 3D hydrogels.

Finally, we integrated the MI-device with a 3D *in vitro* mucus model (see Paragraph 3.3). This integrated system overcame some limitations posed by *in vivo* models when investigating the specific role of LPS in the microbiota-gut-brain axis, as well as the lack of standard *in vitro* tools that accurately replicate the bioinspired structure of the gut barrier.

3.1. Optimization of the intestinal mucus model I-Bac3Gel

The viscoelastic properties of the intestinal mucus were reproduced by alginate-based hydrogels (I-Bac3Gels), as previously reported [75]. The transfer of the reproduced mucus to the MI-device required peculiar challenges. Among these, the stability of the model for a proper time-frame, in the same culture medium used for the target culture, is a prerequisite to avoid changes in the structural feature of the system or to avoid the release of unwanted degradation products that may represent confounding agents in the characterization of either physical (like diffusion of molecules) or biochemical (like production of molecules) phenomena. In the case of I-Bac3Gel, the model resulted stable in the DMEM culture medium as the maximum weight loss was observed after 21 days of immersion and was lower than 10 % (equal to the ~ 6 %) of the initial weight (Fig. 2 A).

The I-Bac3Gels recapitulated the features of the physiological mucus, as the frequency response of the I-Bac3Gel was comparable with hydrogel-*like* behaviour, and the storage modulus G' was higher than the loss modulus G'' for all the frequency spectra considered (Fig. 2 B). At the physiological frequency of the migrating motor complex (0.1 Hz), the storage and loss moduli were equal to 80 ± 19 Pa and 7 ± 2 Pa, respectively.

The microstructure of the mucus models, that plays a key role in the definition of the mass transport through a matrix either of biological or artificial origin, was evaluated by means of a rheological approach. The viscoelastic properties (G' and G'') were successfully fitted by the GMM (Fig. 2C) by error minimization, resulting optimal when 4 Maxwell elements were considered for the fitting (Table 1). In this case, the G' and G'' obtained from the model were found to be comparable to the experimental data and equal to 83 ± 19 and 6 ± 1 Pa, respectively. The shear modulus and mesh size, estimated by coupling the fitting parameters of the 4-elements GMM with the elasticity rubber theory and the hypothesis of an ideal polymeric network, were equal to 107 ± 24 Pa and 41 ± 3 nm, respectively.

The evaluation of the I-Bac3Gels to allow the release of molecules was performed by including a fluorescent dye in the mucus matrix and by studying its release. In particular, the production protocol was modified to incorporate LPS-FITC during the preparation of the hydro-

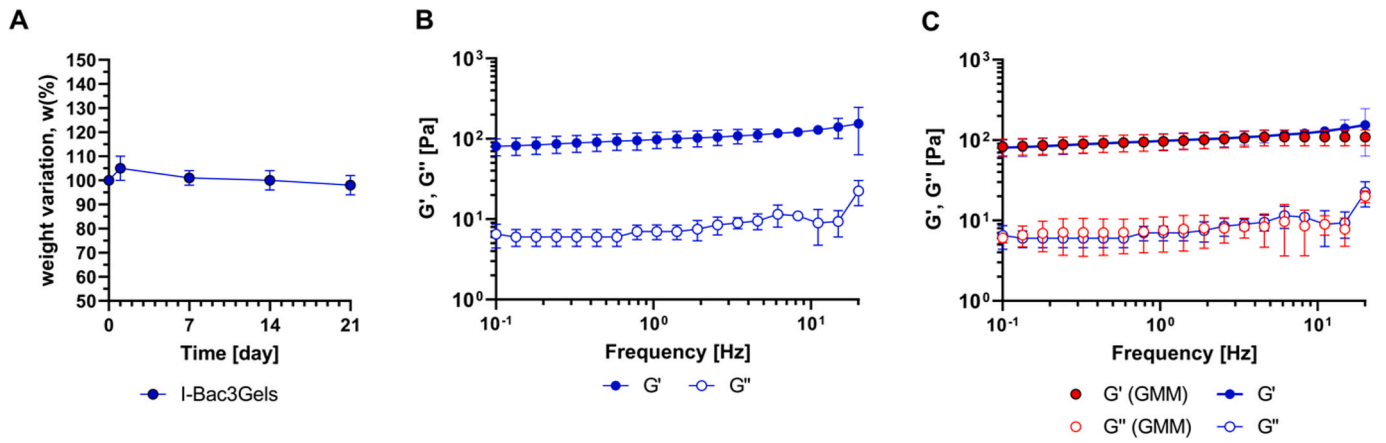

Fig. 2. A) Stability of the intestinal mucus model in a time period of 21 days. B) Viscoelastic properties of the model expressed in terms of storage (G') and loss (G'') moduli in the frequency spectra of 0.1–20 Hz. C) Generalized Maxwell model results fitting (red colour) the experimental data (blue colour). (Data obtained by three independent experiments with n = 5).

Table 1
Shear modulus of the elastic element of the GMM that were obtained to estimate the shear modulus and the mesh size of the alginate-based intestinal mucus model.

G_e [Pa]	G_∞ [Pa]	ξ [nm]
80 ± 19	107 ± 24	41 ± 3

gel. This change did not impair the gel formation, as qualitatively investigated by the inverted tube test. The release of the LPS-FITC was time dependent (Fig. 3 A), and reached the concentration of 42 μg/mL at plateau after ~ 300 min. The rate of release (expressed as %) was successfully described by the Weibull models (Fig. 3 B) as expressed by the formula:

$$\frac{M(t)}{M(\infty)} = \left(1 - e^{(-a \bullet t)^b}\right) \cdot 100$$

where $M(t)$ is the mass of the molecules diffused at the time t, $M(\infty)$ the mass of diffused molecules at the equilibrium, and a and b the fitting parameters. By minimizing the chi-squared error, it was possible to identify the best fitting parameters of the model (*i.e.*, $a = 0.02$, $b = 0.87$), indicating that the 50 % of the mass transport phenomena were exhausted after 69 min, the 75 % after 142 min and the 90 % after 245 min.

To validate the I-Bac3Gels from both the biological and functional point of view, two different strains of *E. coli*, as representative strains of the bacteria consortium composing the human microbiota, were selected to investigate the capability of the mucus model to sustain bacterial growth. The availability of ATCC or CCUG *E. coli* strains was independent from the culture condition, as the planktonic suspension (pK) or the presence of the 3D hydrogel (3D) lead to comparable CFUs for each time point and membrane considered. For example, the differences between the CFUs of the ATCC and CCUG *E. coli* cultured in 3D vs pK was 3 and 5 %, respectively, after 24 h of (T) culture (Fig. 4 A and C).

The availability of ATCC *E. coli* was time-dependent (Fig. 4 B), with a reduction of the bacteria concentration either in the culture in suspension or within the 3D mucus model: from ~ 4.9 to ~ 1.5 ± 0.9 · 10^9 bacteria/mL and from ~ 5.1 to ~ 0.9 · 10^9 bacteria/mL, respectively. Differently, the other conditions were not influenced by the time, as the concentrations obtained in the static culture were comparable for each time point (*e.g.*, from ~ 1.5· 10^9 bacteria/mL at 24 h to ~ 1.3 · 10^9 bacteria/mL after 72 h in case of CCUG 3D cultured with translucent membrane) (Fig. 4 D).

The concentration of LPS was quantified (Fig. 5) to evaluate the possible effect of the 3D environment on the bacteria behaviour. The validity of the LAL in case of the 3D condition was confirmed by preliminary investigation, as no interferences between the sterile hydrogels and LAL negative control were found in the absorbance at 407 nm, as

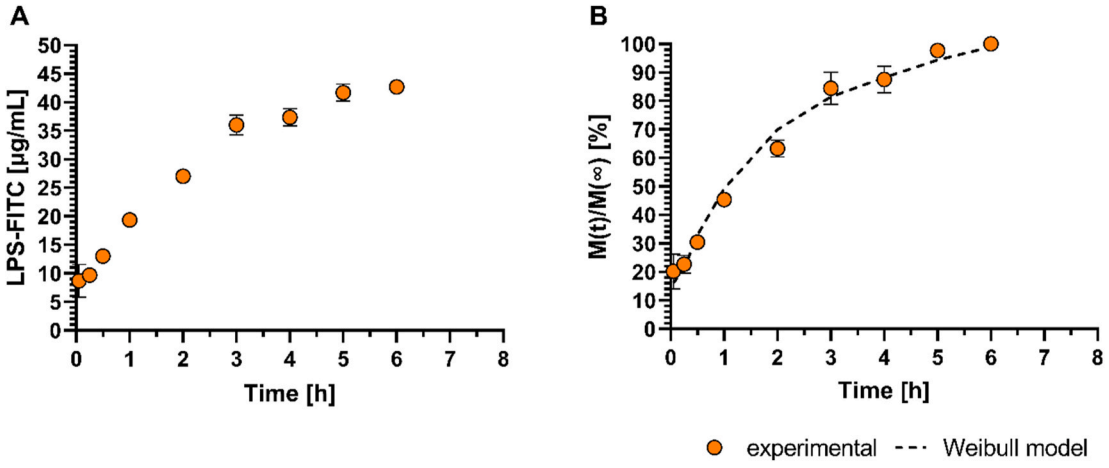

Fig. 3. A) Release profile of the LPS-FITC from the I-Bac3Gel to the medium in time. B) Release rate of the LPS-FITC and the Weibull model fitting the experimental data. (Data obtained by three independent experiments with n = 5).

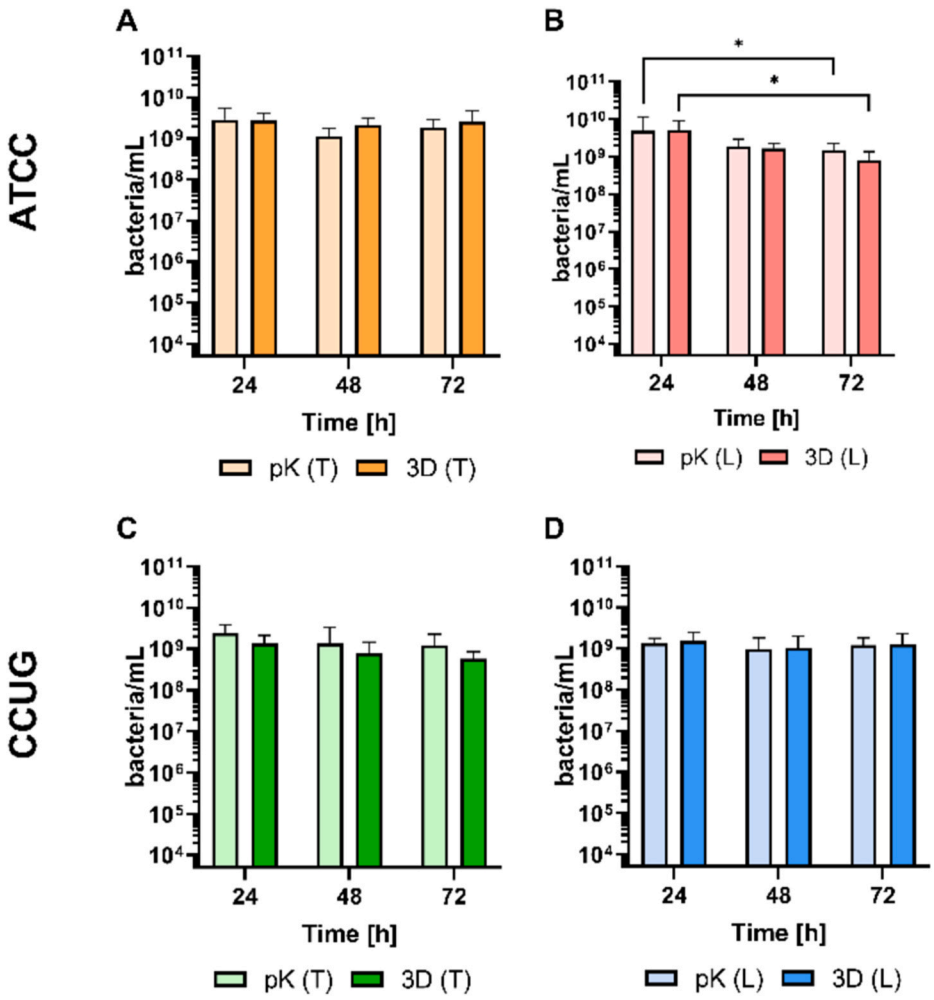

Fig. 4. Viability of ATCC and CCUG *E. coli* (A-B and *C*-D respectively) after being cultured in the I-Bac3Gel (3D) or suspension (pK) for different time periods (24, 48 and 72 h) in Transwell-*like* insert with transparent (T) or translucent (L) PET membranes to separate the hydrogels from the medium. (Data obtained by five independent experiments with n = 3).

defined by the manufacturer instruction.

The type of culture, in suspension (pK) or in I-Bac3Gels (3D), greatly influenced the production of LPS. The LPS produced were higher in case of static 3D culture either for ATCC or CCUG *E. coli* cultured with transparent (T) or with translucent (L) membrane. These differences were maximum in case of ATCC *E. coli* (T) after 24 h of culture, with the 3D condition inducing an increase of the concentration of LPS by a factor of 20 (Fig. 4 A). Oppositely, the minimum difference was measured for CCUG *E. coli* (T), where the pK-related concentration of LPS was equal to the 84 % of the 3D culture (Fig. 5C).

The production of LPS was generally directly associated with time. Indeed, the concentration of LPS was found minimum, for all the conditions considered, after 24 h and maximum after 72 h. However, for the cultures performed with transparent membranes, the increase of the concentration of LPS became significant only after 72 h of culture for both ATCC and CCUG strains.

For a fixed strain (ATCC or CCUG) and culture condition (pK or 3D), the concentration of LPS found in the medium was highly dependent from the type of membrane used (T or L) to separate the I-Bac3Gels from the sterile medium. The transparent (T) membranes were indeed associated with lower endotoxin concentration, while the translucid (T) membranes facilitated the diffusion of LPS. For example, in the 3D culture of ATCC (24 h), the concentration of LPS changed from 38 ± 13 ng/mL to 725 ± 32 ng/mL in case of T and L membrane, respectively. This represented also the maximum difference found between the T and L cultures in absolute (*i.e.*, increase of factor of ~ 19). Differently, the T and L condition that expressed the lowest difference in the concentration of LPS was the ATCC *E. coli* cultured in suspension (pK) for 24 h, where the concentration of LPS was equal to 24 ± 6 ng/mL (T) and 39 ± 7 ng/mL (L).

The type of strain influenced the concentration of LPS in dependence of the culture condition. Indeed, the use of ATCC or CCUG strains for the culture showed differences generally after 72 h, but not at 48 h, and in case of translucid membrane. For example, the concentration of LPS (72 h) diffused in the medium where translucent membrane was used was equal to 894 ± 81 ng/mL (ATCC) and 962 ± 9 ng/mL (CCUG) for the 3D cultures and equal to 39 ± 7 ng/mL (ATCC) and 150 ± 3 ng/mL (CCUG) for the pK cultures.

3.2. Engineering the MI-device

We have designed the MI-device aiming at producing a dynamic millifluidic system to study the toxicity of LPS, while including an optimized bioinspired mucus model that can actively move in the system.

The design of the MI-device (Fig. 6) sustained a wide range of medium inflow as no leakage of distilled water was observed for all the flow rates considered from 0.5 to 400 μL/min. The vaporized hydrogen peroxide resulted to be an efficient method to avoid unwanted infections. The undiluted samples of the medium that flowed into the

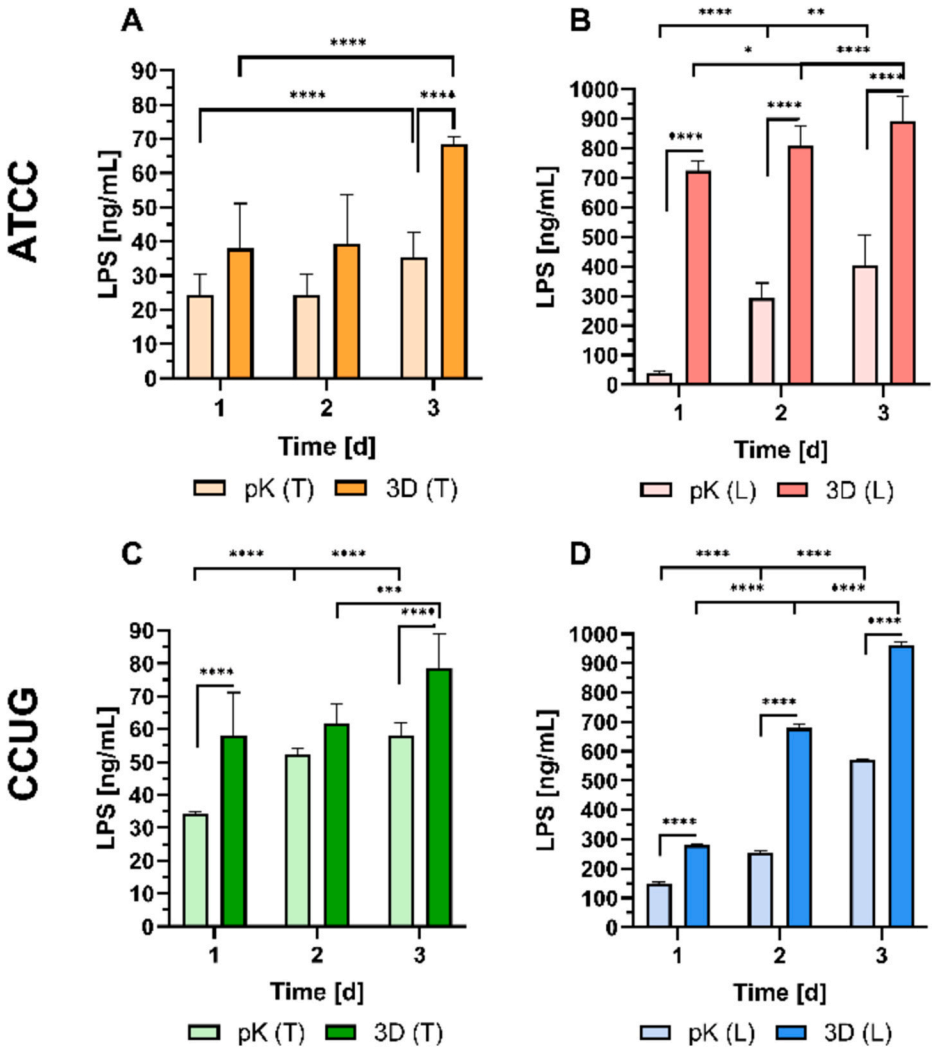

Fig. 5. Concentration of LPS quantified in the medium added to the insert with transparent (T) or translucent (L) membrane in contact with ATCC (A and B) or CCUG (C and D) *E. coli* cultured in suspension (pK) or within the intestinal mucus model (3D). (Data obtained by five independent experiments with n = 3).

device, collected in different points of the system, did not lead to visible bacteria growth onto the LB-agar plates.

The main criteria used for designing the MI-devices were:

1. Possibility to allow the flow of I-Bac3Gels infected with bacteria;
2. Possibility to extract sterile medium for the quantification of LPS;
3. User-friendly assembly.

The presence of an elliptical base in the basal hemi-chamber facilitated the I-Bac3Gel flow, that was easily conveyed from the inlet tube to the outlet without bubble formation or leakage of the mucus model (Fig. 6). The presence of a commercially availabe insert as a third and removable element of the MI-device had different aims. First, it acts as a separation element between the basal and the apical hemi-chamber, impairing bacterial motion from the I-Bac3Gels to the medium, while providing porosity for the diffusion of the molecules (*e.g.*, LPS) to be quantified. Secondly, it makes the dynamic culture performed in the MI-device comparable to standard static bacterial culture made in 6-well Transwell-*like* multiwell plate, which can hence be used as a control configuration.

3.3. Integrating the MI-device and the I-Bac3Gels

The bacterial concentrations were comparable in the different dynamic culture conditions at a fixed time point (Fig. 7), as the type of membrane used (T or L) and the *E. coli* strains (ATCC or CCUG) resulted in comparable CFUs number after 24, 48 and 72 h. The maximum concentration of bacteria was reported for the 3D dynamic culture of ATCC with translucent insert (dyn3D (L)) after 24 h, while the 3D dynamic culture of CCUG *E. coli* cultured with transparent interest for 72 h showed the lower bacterial concentration, that was decreased by 76 % (from $3.0 \pm 1.5 \cdot 10^9$ to $7.3 \pm 2.6 \cdot 10^8$ bacteria/mL).

Differently from the experimental set-up conditions, time had a role in the bacterial concentration measured in the dynamic culture in specific condition. Although the 3D dynamic culture of CCUG strain was not influenced by time, the ATCC showed a decrease of about 27 % from 24 to 72 h in the bacterial concentration (from $1.2 \pm 0.2 \cdot 10^9$ bacteria/mL to $8.7 \pm 2.9 \cdot 10^8$ bacteria/mL) in case of transparent membrane (T), while remaining comparable in case of translucent membrane (L) ($\sim 3.0 \cdot 10^9$ bacteria/mL).

Importantly, the dynamic stimulation did not impair the growth of bacteria, as no differences were observed between the 3D dynamic culture, mounted with either transparent or translucent inserts, of both ATCC and CCUG *E. coli* and the correspondent static 3D control.

The design of the MI-device was suitable for the collection of sterile LPS in the apical hemi-chamber and allowed its post-culture quantification, as the medium of the apical hemi-chamber was found sterile in all the experiments performed, independently from the insert type and

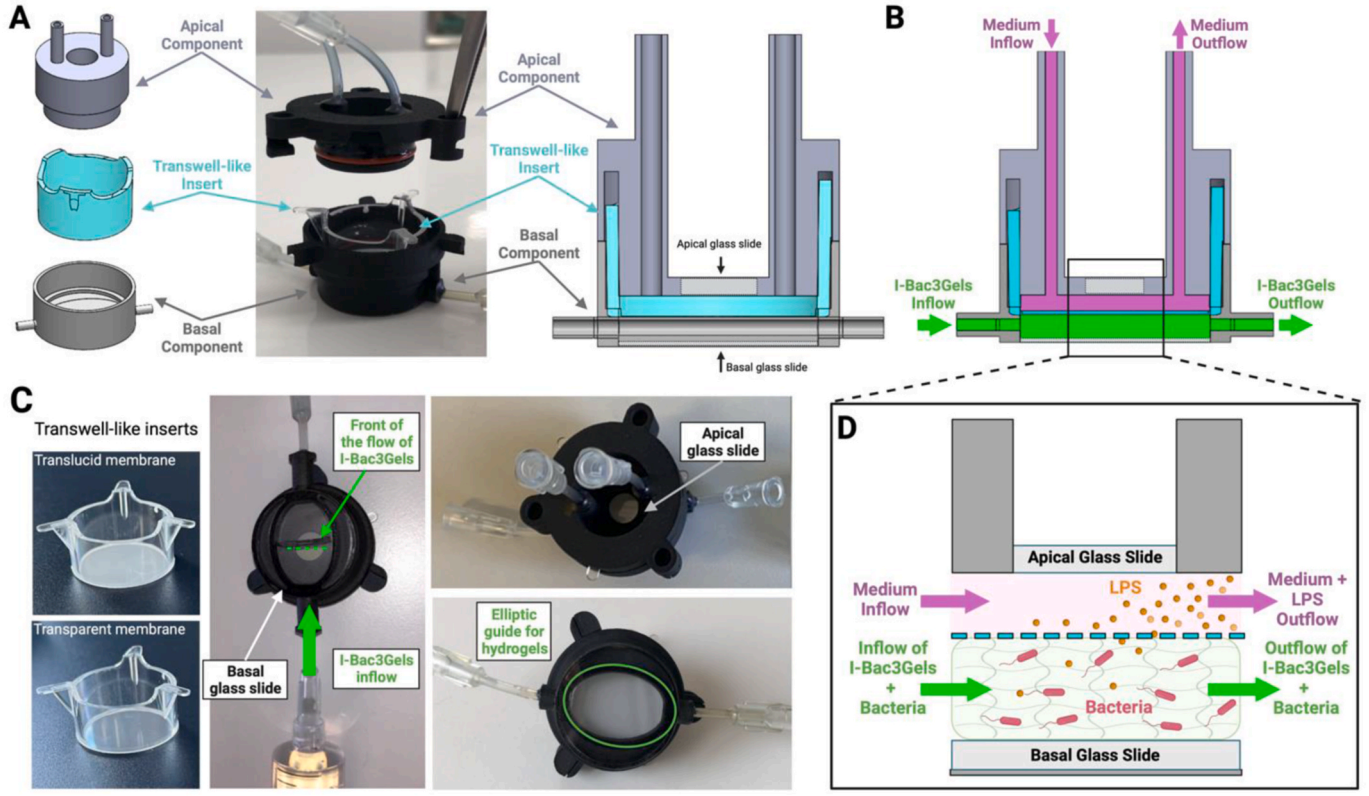

Fig. 6. Design of MI-device for 3D dynamic culture of bacteria. (A) Exploded and combined vision of the three components (apical and basal components and Transwell-*like* insert) composing the MI-device. B) Assembled MI-device with red and blue colours representing the fluid dynamics of the apical and basal hemi-chambers, where the flows of culture medium (red, apical hemi-chamber) and of I-Bac3Gels (green, basal hemi-chamber) are separated by the membrane of the Transwell-*like* insert (in blue). C) Real pictures of the Transwell-*like* inserts and of the MI-device (bottom and top visions) showing the pre-filling inflow of the I-Bac3gels. D) Focus on the functional area of the MI-device where the exchange of molecules occurs. The I-Bac3Gel with the embedded bacteria flows in the basal hemi-chamber. Thanks to the porous membrane, the bacteria-derived molecules, including LPS, can diffuse into the apical hemi-chamber (for technical and dimensional details, see Refs. [80–82]) and can be collected for further use.

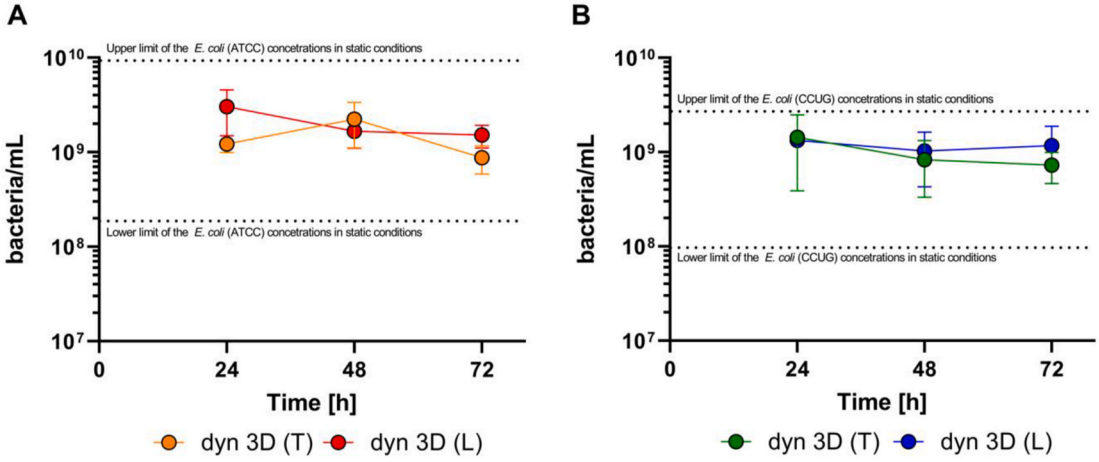

Fig. 7. 3D dynamic culture of ATCC (A) and CCUG (B) cultured in the MI-device mounted with transparent (T) or translucent (L) commercial inserts. The dashed lines represent the upper and lower ranges of CFUs counted for 3D static culture for ATCC (left) and for CCUG (right). (Data obtained by five independent experiments with n = 2).

bacterial strain.

The diffusion of LPS was affected by the experimental set-up, strain and time (Fig. 7). At a fixed time and *E. coli* strain, the LPS diffused in the medium through the translucent membrane were higher than the ones diffused through the transparent membrane by near one order of magnitude in case of ATCC *E. coli* and by a factor of 6 in case of CCUG *E. coli*. Moreover, comparing the cultures between the two strains, differences in the concentration of LPS were found only in case of translucent insert (L) at 24 and 48 h, with the ATCC *E. coli* reaching up to ~ 3 and ~ 2 times the concentration of LPS produced by the CCUG *E. coli*. After 72 h of culture, the LPS derived by ATCC and CCUG *E. coli* resulted comparable.

The passing of time was related to an increase of the concentration of LPS in the fresh medium of the apical hemi-chamber. Independently from both the type of insert (T or L) and the strain (ATTC or CCUG), the concentration of LPS quantified after 72 h of culture was higher than the one quantified after 24 h. For example, the 3D dynamic culture of ATCC *E. coli* cultured in the MI-device mounted with a translucent insert (L) increased by 150 % from 24 to 72 h (from 1137 ± 100 ng/mL after 24 h to 1785 ± 91 ng/mL after 72 h). Similarly, the concentration of LPS produced by CCUG *E. coli* cultured in the same condition (insert L) after 24 and 72 h of culture increased by 386 % (423 ± 34 and 1636 ± 42 ng/mL).

The dynamic stimulation greatly enhanced the production of LPS (Fig. 8). Indeed, both ATCC and CCUG *E. coli* cultured in 3D dynamic condition showed an evident increase of the concentration of LPS in the medium of the apical hemi-chamber compared to the static culture. The maximum difference, in particular, was observed in case of ATCC cultured for 48 h in the MI-device mounted with transparent insert, that exhibited a concentration of LPS in the dynamic culture 4.5 time higher than the static culture with the same type of insert (39 ± 14 and 179 ± 27 ng/mL for 3D dynamic and static culture, respectively). Differently, the minimum difference was found in case of CCUG *E. coli* cultured in 3D dynamic and static condition, where the concentration of LPS was equal to 851 ± 59 and 680 ± 12 ng/mL, respectively (*i.e.*, lower by a factor of ~ 1.2).

To evaluate the biological impact of the bacteria conditioned media containing LPS generated in the MI-device, the medium derived from the dynamic 3D culture of ATCC *E. coli*, was collected and employed for the treatment of statically cultured Caco-2 cell monolayer. After a treatment period of 11 days, we noticed a significant impact on the integrity of the Caco-2 monolayers (Fig. 9). Although morphology was comparable for treated and untreated samples, the TEER measurement of the Caco-2 cell monolayers subjected to the enriched culture medium exhibited a lower value if compared to the monolayers cultured in standard culture medium. Specifically, the TEER of the treated Caco-2 cells was recorded at 394 ± 37 Ω cm^2 after 11 days, reflecting a 21 % reduction in the TEER when compared to the TEER values of the untreated samples (*i.e.*, 499 ± 69 Ω cm^2). This reduction of cellular layer integrity persisted in the subsequent time points, with a 15 % decrease in the TEER of the final day of treatment (day 21) for the treated Caco-2 cultures (382 ± 8 Ω cm^2) in comparison to the untreated control group (447 ± 34 Ω cm^2).

4. Discussion

The human gut microbiota dialogues with the intestinal tissue by a complex biomolecular alphabet [17,18,83]. Different approaches can be exploited to answer multiple questions: direct co-culture of cells and bacteria are powerful tools to evaluate the role of specific biological actors in target pathological scenarios. Similarly, the separation of biological actors can allow the manifestation of unknow mechanism that are masked into complex systems [20,84,85]. This work is inserted in the second approach: our scope is to provide tools that are suitable for disassembling the complexity of the mechanism used by bacteria to affect cells.

Gut-on-a-chip devices successfully investigated different aspect of

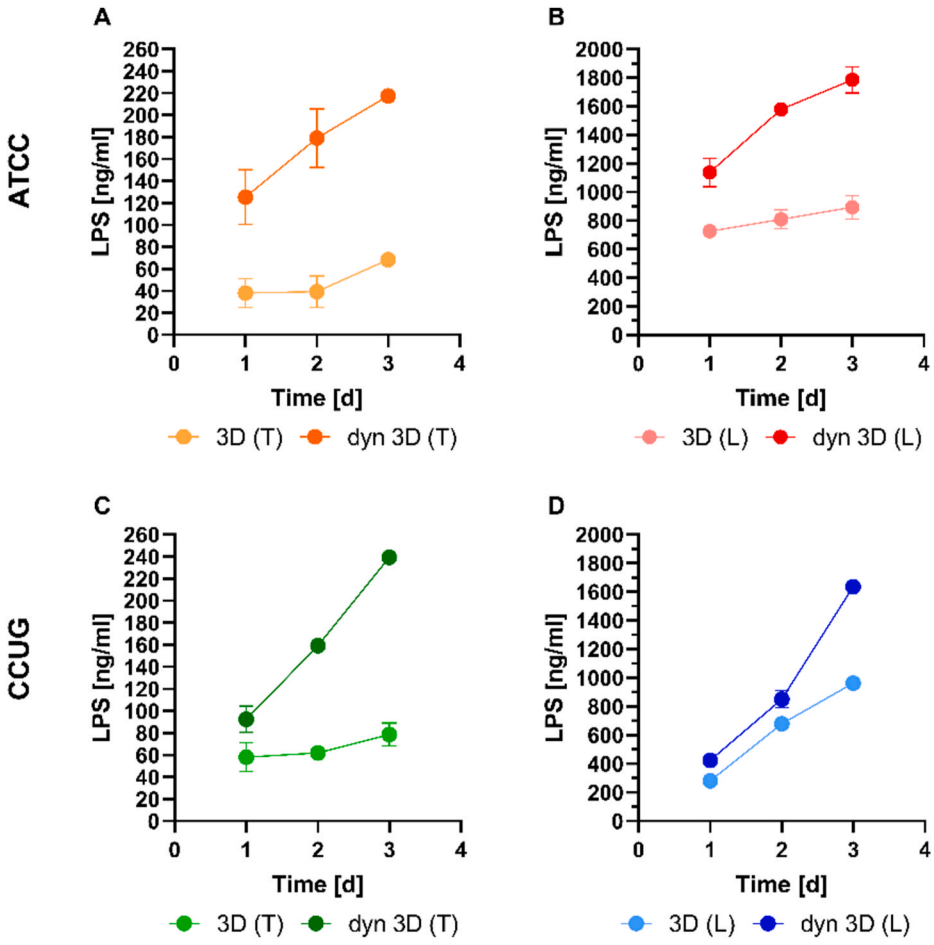

Fig. 8. Concentration of LPS quantified in the apical hemi-chamber of the MI-device mounted with transparent and translucent (T and L, respectively) inserts for the 3D dynamic culture of ATCC (A and B) or CCUG (C and D) *E. coli*. The concentration of LPS of the 3D static cultures (3D(L) and 3D(T)) were reported for comparison. (Data obtained by five independent experiments with n = 2).

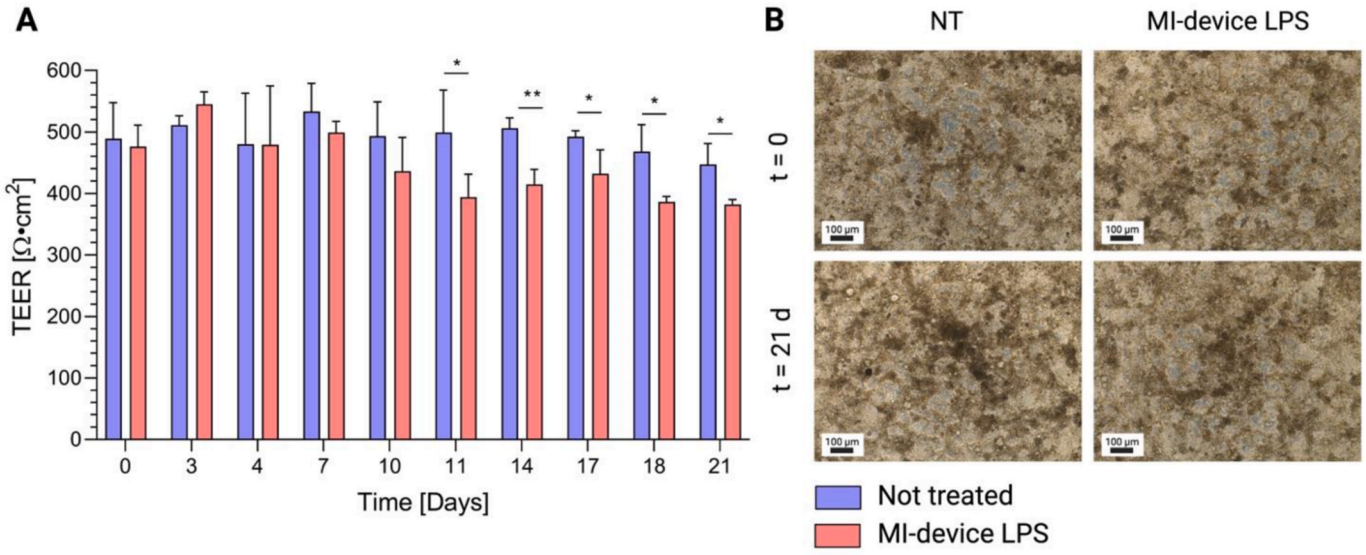

Fig. 9. Effect on Caco-2 cells of the LPS-containing medium obtained by 3D dynamic culture of ATCC *E. coli* in the MI-device after 72 h. Integrity and morphology of the epithelial cell monolayer were measured respectively by means of TEER quantification (A) and light microscopy (B) (representative picture, scale bar of 100 μm). (Data obtained by two independent experiments, each assessed in triplicate).

this crosstalk by co-culturing human gut cell-based models with bacteria and evaluating biological parameters like TEER and permeability [21,86,87]. However, gut-on-a-chip devices are not specifically designed to control the production, the extraction and the quantification of bacteria-derived molecules that are at the base of the biological response. This aspect is still a challenge. For this reason, we engineered a new flexible dynamic system, the MI-device, conceived to control the production and the mass transport of bacteria-derived molecules in a physiological-*like* microenvironment (*i.e.*, *in vitro* mucus model I-Bac3-Gels) during its dynamic motion.

The design of the MI-device comprehends one basal and one apical hemi-chamber, acting as a source and a collector point respectively of the molecules that enrich the medium flowing into the system (Fig. 6 B). Molecules diffuse from the basal to the apical hemi-chamber through a separating PET membrane, provided by a commercially available Transwell-*like* insert. The three different components, *i.e.* two custom-made units and the Transwell-*like* insert, are assembled (Fig. 6 A) in a user-friendly process, not requiring screws and other supporting equipment, without impacting the hydraulic sealing, bacterial penetration and flow separation in between the two hemi-chambers.

The presence of the additional element in the design brings different advantages. For instance, the Transwell-*like* insert can be extracted and re-inserted in the MI-device during the dynamic culture, providing samples representative of the *in-situ* condition of the apical chamber after interruption of culture medium flow. This aspect is particularly important in the characterization of the mass transport of target molecules, as it allows to have a punctual measurement of the concentration of the molecules in the area where the diffusion process directly takes place and not downstream it (*i.e.*, in the reservoirs). In the reservoirs, the concentration of the molecules can be assumed as comparable to that in the chamber only with proper experiment management, for example by limiting the culture to short periods in order to avoid excessive sample dilution and/or by frequently changing the reservoirs [88]. Moreover, the similarity between the dynamic system and the static controls, both including the same Transwell-*like* insert, is improved with respect to the systems where the separating membrane in the dynamic system is customized accordingly to the specific design of the device, that may differ from the static condition (typically a Transwell®) and makes more complex the comparison with the control cultures [62].

The final aim of the MI-device is to provide a bioinspired tool including a gut mucus model to target the molecules produced by bacteria that are relevant for the microbiota-gut crosstalk. The intestinal mucus is generally inserted inside the gut-on-a-chip through hydrogels, deposited in the form of films, that are static and without their own dynamic motion inside the device, on membranes separating the various compartments of the system [64,89–92].

The MI-device introduced an innovative approach to include the gut mucus in a dynamic system: dynamism and 3D-bioinspired structure were considered as intertwined aspects to be modelled in order to recapitulate the functionality of the intestinal barrier. For this reason, the MI-device was designed with the basal hemi-chamber with an elliptical base and a silicon O-ring to convey the 3D hydrogel-based mucus model, dynamically moving in the system, towards the reservoirs without inducing leakage and unwanted bacterial penetration as demonstrated by the hydraulic sealing (flowrates up to 400 μL/min) and agar-plates contamination evaluation.

In order to include a model that effectively simulates the barrier characteristics of the intestinal mucus, two key aspects that determine the mass transport of molecules towards the gut epithelium were taken into account: the viscoelastic properties and the mesh size of the polymeric network within the mucus [93,94].

Considering the perspective of using the MI-device in culture condition with the presence of eukaryotic cells, the I-Bac3Gels were produced in DMEM and the hydrogel formation achieved by crosslinking alginate with insoluble calcium salts and an acidifying agent to reach homogeneous properties [75,77,95–97]. The formulation here proposed showed an elastic-*like* predominant behaviour ($G' > G''$), expressing viscoelastic moduli in the physiological range of reference (2–200 Pa) (Fig. 2-A) [56]. Similarly, the Generalized Maxwell Model was adopted as method to estimate the shear modulus G of the engineered mucus model and then to compute its mesh size, exploiting the elastic rubber theory, thus get greater insights over the final microstructure (Fig. 2C and Table 1) [60,76]. Importantly, the model displayed similar ξ (41 ± 3 nm) when compared to physiological loose mucus layer mesh size (30 nm) [54].

The combination of proper viscoelastic properties with biosimilar mesh size resulted in a successful diffusion of LPS-FITC as a model molecule of LPS directly produced by bacteria over time (Fig. 3 A). However, to model the biomolecular crosstalk between bacteria and cells, it is fundamental that the mass-transport in the system is comparable to that occurring *in vivo*. For this reason, the biosimilarity of the diffusion was evaluated by the Weillbul's semi-empirical model (Fig. 3

B), where the parameter *b* (see equation (6)) is typically used to describe the type of diffusion occurring in the system [98]. The *b* value (equal to = 0.87) obtained in case of LPS-FITC release is representative of a deviation from the pure Fickian diffusion ($b \leq 0.75$) towards a combination of Fickian and Case II transport type [99]. In this case, a combined effect of viscoelastic relaxation and swelling lead to a facilitated diffusion of molecules in the bulk of the material and a slowing of the front release at the interface with the medium due to surface phenomena [100–102]. Unfortunately, no data are available about the exact type of diffusion occurring *in vivo* in the gut, but a similar behaviour was reported in animal studies where the diffusion of molecules was facilitated in the loose mucus layer and reduced in the attached one [103,104].

The release of a commercially available LPS-FITC is an indicator of the suitability of the bioinspired mucus model to act as an intermediator between bacteria and cells. However, viable bacteria and production of bacteria-derived LPS are *sine qua non* prerequisites to reproduce in the MI-device the *in vivo* biomolecular dialogue between the microbiota and gut. For this reason, two different *E. coli* strains (ATCC and CCUG), used in other studies for the evaluation of the toxicity of LPS either *in vivo* or in a gut-on-a-chip device [63,105,106], were selected in this work as proof of concept and simplified models of LPS-producing bacteria present in the human microbiota.

The MI-device supported the growth of bacteria in a 3D dynamic microenvironment in movement into the system. The 3D dynamic culture of bacteria was engineered by two technical aspects: first, the elliptical shape of the base allowed the motion of the mucus model, infected by the selected bacteria, without blockage of the inlet and outlet of the basal hemi-chamber. Second, the chambers were designed to maximize the exchange of molecules between the chambers through the Transwell-*like* insert membrane (area 452 mm^2) by imposing the smaller radius of the ellipse equal to the radius of the insert. This resulted in a sufficient nutrients availability to maintain a viable bacterial population with concentration ($\sim 10^9$ bacteria/mL) comparable to the static condition, independently from the *E. coli* strain considered (Fig. 7). Importantly, it was observed that the addiction of two level of complexity towards a more *in vivo-like* culture, *i.e.* the 3D microenvironment and the dynamic motion, corresponded to comparable bacterial concentration that was reached when using the standard method of culturing bacteria (*i.e.*, suspension) (Fig. 4).

The presence of a bioinspired intestinal mucus model was a key element enhancing the availability of LPS. Indeed, the presence of the tridimensional network increased the concentration of LPS up to 3,2 times (Fig. 5) compared to the culture condition performed in liquid at each time point and independently from the *E. coli* strain considered. Since the 3D culture condition was not related to an increased bacterial concentration and the mucus model was produced with the same culture medium of the suspended cultures, it was hypothesized that the increase in the availability of LPS derived from a physical-mechanical effect of the 3D structure on the bacterial body. This hypothesis is supported by the already-reported evidence that the detachment of LPS from the bacterial wall is linked to shear forces (*e.g.*, arising during motility), although no specific studies were performed to explain the mechanism behind this process [107,108]. The results of this work are, therefore, further evidence of how the type of the environment, such as solid-*like* vs liquid-*like* state, has a deep impact on the production of LPS, similarly to what has already been described for other aspects of bacterial behaviour, such as adhesion, drug tolerance, gene expression and increased protein production [109–111].

The application of dynamic stimulation in the MI-device further favoured the production of LPS (Fig. 8). The influence of the bioinspired microenvironment of the mucus model and the dynamic motion occurring in the basal hemi-chamber cooperated synergically to induce a great increase of the concentration of LPS in the apical chamber, ranging from 150 % to 350 % with reference to the static condition (Figs. 5 and 8). During the 3D dynamic culture of bacteria in the MI-device, the physical effect of the 3D environment on the bacterial wall, and hence on production of LPS, was combined with the further stimulus of the dynamic motion and the continuous turnover of the bacterial population in the area of the membrane governing the mass-transport phenomena between the chambers. These aspects were considered at the base of the increased production of bacteria-derived molecules such as lipids, nattokinase, cyclic adenosine monophosphate, cellulases and other molecules in bioreactors for dynamic (non-3D) culture of bacteria [112–114].

The availability of target molecules is a necessary but not sufficient aspect to engineer a new tool to model *in vitro* the biological communication between bacteria and cells. After being produced, the molecule quantification through specific analytical assays is required to characterize these processes. Typically, these assays use a minimal sample volume and/or a series of post-culture manipulation [115]. A too low working volume of the system, although minimizing the costs and maximizing the cell density, imposes a careful selection of the characterization technique of the culture. For example, few microliters of working volume make difficult or time dispending the obtainment of the minimal sample quantity for the serial dilutions needed for the CFU counting. For this system, a more complex characterization, like live-dead assays, could be required for bacteria viability investigation [116]. Similarly, low volume samples are not compatible with the selected techniques for the quantification of LPS (< 100 μL in case of LAL) [117]. This is because, if bacteria are present in the sample, it needs to be further filtered before the assay is started, lowering even more the final available sample size.

The versatile design of the MI-device overcame these limits and the concentration of LPS was always found detectable in all the experiment performed (Figs. 5 and 8). The concentration of LPS in the receiving chamber is governed by the volume ratio of the two hemi-chambers, the pore density of the separating membrane and the flowrates of the culture media. Specifically, the apical/basal chamber volume ratio was designed to be 1:1, as previously reported [21,22,118] but at a larger scale (∼ 2 mL). The availability of LPS in the MI-device is further enhanced by preventing the passage of *E. coli* from the basal to the apical hemi-chamber though the separating membrane with a pore dimension of 0.4 μm for both translucent and transparent Transwell-*like* inserts. Devoid of bacteria, the entire volume of the apical hemi-chamber is ready-to-use for the downstream quantification of LPS and not susceptible to sample loss derived, for example, by filtration or centrifugation processes.

In this study, we considered LPS as it is a well-characterized molecule having an impact on the gut barrier properties in different pathophysiological scenarios [43–45]. However, the easy control over the pore dimensions and density of the separating membrane, and the complete hydraulic separation of the two hemi-chambers make the MI-device suitable for the study not only of LPS but also of other bacteria-produced molecules. It is possible to change the filtering power of the membrane, for example by increasing the pore density, and to tune the flow of the apical hemi-chamber, for example by imposing a lower flowrate, thus optimizing the accumulation of molecules that may differ in terms of diffusivity in comparison to LPS.

The control of the mass-transport of molecules is an advantage in the *in vitro* modelling of biological phenomena where the diffusion processes are a key aspect [84,119,120]. It is indeed possible to shift from a condition at lower concentration, modelling a physiological-*like* state, to one at higher concentration, representative of a pathological-*like* state, by changing only one component of the set-up, while keeping the production process of the model unchanged. In the specific case of the toxicity of LPS, no local gut values considered as physiological are reported in the literature, but only the systemic concentration measured by plasma analysis (order of magnitude of picograms) [40,41]. The lack of a local reference makes difficult to evaluate the toxicity of LPS *in vitro*, and consequently different endotoxin concentrations were used to treat the Caco-2 cell monolayer [46–48].

It is worth noticing that the facilitated diffusion of LPS over time in the MI-device is within the concentrations range of LPS used in different

studies [121–123]. In particular, the change from a transparent (pore density of $2{\cdot}10^6$ pores/cm^2) to a translucent (pore density of $1{\cdot}10^8$ pores/cm^2) Transwell-*like* insert leaded to an increase of the concentration of LPS of one order of magnitude (Fig. 8), reaching the same concentration ($\sim$ 1 μg/mL) that was reported to quadruplicate the permeability in Caco2-cell monolayer, as well as an increased expression of different proinflammatory molecules [34,120–124].

It was important to assess if the MI-device is a suitable tool to study the effect that bacteria-derived molecules have on gut cells in a perspective view to study more complex phenomena like the microbiota-gut-brain axis. For this reason, a 3D dynamic culture was performed culturing ATCC *E. coli* and mounting the device with translucid (L) Transwell-*like* insert, as this set up was shown to yield the concentrations of LPS comparable to those found to be biologically active [39,124,125].

The MI-device successfully produced an LPS-containing culture medium exhibiting quantifiable biological effects on the epithelial cells. After 11-days of treatment period, it was indeed possible to observe a reduction in the integrity of the Caco-2 cells, with a decrease in TEER between 15 % and 20 %, consistent with other experimental data showing a time-dependent effect of LPS and comparable TEER values [48,80].

Interestingly, the effect of the LPS produced in the MI-device resulted in the loss of functional integrity, a critical aspect implicated in various pathological phenomena, including leaky gut, inflammatory bowel disease , and as hypothesized in the context of the gut-brain axis.

Even if we are not able to exclude that other *E coli* derived molecules besides LPS acted on Caco-2 cells, we demonstrated that the MI-device successfully generated an LPS-containing culture medium with a concentration of LPS that is suitable to detect a biological response in the gut cells, even though further experimental confirmations may be needed to get insight into these phenomena.

The possibility for the MI-device to perform 3D dynamic culture of bacteria producing molecules of interest, and to enable their quantification represent advantages that are, in principle, ready to be applied in both stand-alone or integrated systems.

As a stand-alone system, the MI-device makes available molecules of interest, that are directly produced by bacteria within a 3D bioinspired structure dynamically moving in the system. The sterile extraction of these molecules, diffusing from the basal to the apical hemi-chamber, enable their quantification without the need for additional filtration step. This advantage makes, in principle, the MI-device also feasible to be integrated in-line with other dynamic devices, specifically tailored for eukaryotic cultures, including Caco-2 cells [19,24,80,91,92,126]. In both the approaches, the MI-device can hence contribute to the advance of our understanding of complex biological phenomena, either in a physiological or pathological scenario, like the microbiota-gut-brain axis, that are not yet completely characterized.

5. Conclusion

Direct co-culture of cells and bacteria is a potent method for evaluating the biological role of LPS in targeted pathological scenarios, also related to the gut-brain axis. Synergically, the separation of bacteria from cells can instead contribute to study the hidden mechanisms through which bacteria-derived molecules like LPS carry out their action on eukaryotic cells.

This work provides a tool for disassembling some aspect of the complexity of the bacteria-cells molecular dialogue. We engineered a new technological tool, the MI-device, that integrated a user-friendly and easy-to-control design with the presence of a bioinspired *in vitro* mucus model representing the microenvironment where the bacteria-host tissue crosstalk is performed.

The MI-device meets the need of a gut-on-a-chip approach (*i.e.*, dynamic stimulation) featuring also the *in vitro* modelling of the intestinal mucus, proving to be a useful tool to assess relevant aspects of the not-yet completely characterized impact of bacteria on human health and diseases. The synergy between MI-device and I-Bac3Gels empowered the production of LPS, as well as their sterile extraction for quantification, thus providing a source of endotoxin that is able to recapitulate *in vitro* a pathological effect on the integrity of human epithelial cells.

The MI-device is ready to be exploited in further studies by both maintaining its stand-alone configuration or by its integration within multi-organ platforms. Other molecules, secreted by other bacterial strains than *E. coli*, can be extracted in the MI-device and quantified during the 3D dynamic cultures. In the future perspective of in-line integration with other dynamic system, the MI-device opens to the possibility of dynamic culture of cells with culture media that are directly enriched with bacteria products, thus mimicking features of selected pathophysiological conditions.

Authors' contributions

LS, PP, DA and CG designed the study; LS wrote the manuscript; LS, MC and LB performed microbiological and biological studies; LS performed the quantification of LPS and data interpretation; FD, LB, FF and SP contributed to the biological experiments; LS and PP designed the I-Bac3Gels to fit the MI-device; LS, MC, LC, FD, SP contributed to the optimization of the MI-device; PP, DA and CG designed the MI-device and supervised the study. All the authors reviewed the manuscript and approved the submitted version; CG funding acquisition.

CRediT authorship contribution statement

L. Sardelli: Conceptualization, Data curation, Writing - original draft. **M. Campanile:** Conceptualization, Data curation. **L. Boeri:** Conceptualization, Data curation. **F. Donnaloja:** Conceptualization, Data curation. **F. Fanizza:** Conceptualization, Data curation. **S. Perottoni:** Conceptualization, Data curation. **P. Petrini:** Conceptualization, Writing - review & editing, Supervision. **D. Albani:** Conceptualization, Supervision, Writing - review & editing. **C. Giordano:** Conceptualization, Data curation, Funding acquisition, Supervision, Writing - review & editing.

Declaration of competing interest

The Authors declare the following financial interests/personal relationships which may be considered as potential competing interests:

Carmen Giordano, Paola Petrini and Diego Albani have a patent related to a device for the culture of biological agents.

Data availability

Data will be made available on request.

Acknowledgements

This study was funded by the European Research Council (ERC) under the European Union's Horizon 2020 research and innovation program (Grant agreement No. 724734-MINERVA). The results reflect only the Authors' views and the Agency is not responsible for any use that may be made of the information contained.

References

[1] J.R. Kelly, C. Minuto, J.F. Cryan, G. Clarke, T.G. Dinan, Cross talk: the microbiota and neurodevelopmental disorders, Front. Neurosci. 11 (2017) 1–31, https://doi.org/10.3389/fnins.2017.00490.

[2] J.F. Cryan, et al., The microbiota-gut-brain axis, Physiol. Rev. 99 (4) (2019) 1877–2013, https://doi.org/10.1152/physrev.00018.2018.

[3] H.X. Wang, Y.P. Wang, Gut microbiota-brain axis, Chin. Med. J. 129 (19) (2016) 2373–2380, https://doi.org/10.4103/0366-6999.190667.

[4] D. Serra, L.M. Almeida, T.C.P. Dinis, The impact of chronic intestinal inflammation on brain disorders: the microbiota-gut-brain Axis, Mol. Neurobiol. 56 (10) (2019) 6941–6951, https://doi.org/10.1007/s12035-019-1572-8.

[5] P.C. Keightley, N.A. Koloski, N.J. Talley, Pathways in gut-brain communication: evidence for distinct gut-to-brain and brain-to-gut syndromes, Aust. N. Z. J. Psychiatr. 49 (3) (Mar. 2015) 207–214, https://doi.org/10.1177/0004867415569801. SAGE Publications Ltd.

[6] E. Patterson, J.F. Cryan, G.F. Fitzgerald, R.P. Ross, T.G. Dinan, C. Stanton, Gut microbiota, the pharmabiotics they produce and host health, in: Proceedings of the Nutrition Society, Cambridge University Press, Sep. 2014, https://doi.org/10.1017/S0029665114001426.

[7] S. Leclercq, et al., Intestinal permeability, gut-bacterial dysbiosis, and behavioral markers of alcohol-dependence severity, Proc. Natl. Acad. Sci. USA 111 (42) (2014) E4485–E4493, https://doi.org/10.1073/pnas.1415174111.

[8] G. Moser, C. Fournier, J. Peter, Intestinale Mikrobiom-Darm-Hirn-Achse und Reizdarmsyndrom, Wien Med. Wochenschr. 168 (3–4) (Mar. 2018) 62–66, https://doi.org/10.1007/s10354-017-0592-0. Springer-Verlag Wien.

[9] H. Tilg, N. Zmora, T.E. Adolph, E. Elinav, The intestinal microbiota fuelling metabolic inflammation, Nat. Rev. Immunol. 20 (1) (Jan. 2020) 40–54, https://doi.org/10.1038/s41577-019-0198-4. Nature Research.

[10] F. Brial, A. Le Lay, M.E. Dumas, D. Gauguier, Implication of gut microbiota metabolites in cardiovascular and metabolic diseases, Cell. Mol. Life Sci. 75 (21) (Nov. 2018) 3977–3990, https://doi.org/10.1007/s00018-018-2901-1. Birkhauser Verlag AG.

[11] E.M.M. Quigley, Microbiota-brain-gut Axis and neurodegenerative diseases, Curr. Neurol. Neurosci. Rep. 17 (12) (2017), https://doi.org/10.1007/s11910-017-0802-6.

[12] L.J. Spielman, D.L. Gibson, A. Klegeris, Unhealthy gut, unhealthy brain: the role of the intestinal microbiota in neurodegenerative diseases, Neurochem. Int. 120 (Nov. 2018) 149–163, https://doi.org/10.1016/j.neuint.2018.08.005. Elsevier Ltd.

[13] S. Roy Sarkar, S. Banerjee, Gut microbiota in neurodegenerative disorders, J. Neuroimmunol. 328 (Mar. 15, 2019) 98–104, https://doi.org/10.1016/j.jneuroim.2019.01.004. Elsevier B.V.

[14] C. Pellegrini, L. Antonioli, R. Colucci, C. Blandizzi, M. Fornai, Interplay among gut microbiota, intestinal mucosal barrier and enteric neuro-immune system: a common path to neurodegenerative diseases? Acta Neuropathol. 136 (3) (Sep. 2018) 345–361, https://doi.org/10.1007/s00401-018-1856-5. Springer Verlag.

[15] T.R. Sampson, et al., Gut microbiota regulate motor deficits and neuroinflammation in a model of Parkinson's disease, Cell 167 (6) (Dec. 2016) 1469–1480.e12, https://doi.org/10.1016/j.cell.2016.11.018.

[16] N.M. Vogt, et al., Gut microbiome alterations in Alzheimer's disease, Sci. Rep. 7 (1) (Dec. 2017), https://doi.org/10.1038/s41598-017-13601-y.

[17] C.R. Martin, V. Osadchiy, A. Kalani, E.A. Mayer, The brain-gut-microbiome Axis, Cell Mol Gastroenterol Hepatol (2018), https://doi.org/10.1016/j.jcmgh.2018.04.003.

[18] T.G. Dinan, J.F. Cryan, Brain-gut-microbiota Axis and mental health, Psychosom. Med. 79 (8) (Oct. 2017) 920–926, https://doi.org/10.1097/PSY.0000000000000519. Lippincott Williams and Wilkins.

[19] I. Raimondi, L. Izzo, M. Tunesi, M. Comar, D. Albani, C. Giordano, Organ-on-A-chip in vitro models of the brain and the blood-brain barrier and their value to study the microbiota-gut-brain Axis in neurodegeneration, Front. Bioeng. Biotechnol. 7 (January) (Jan. 2020), https://doi.org/10.3389/fbioe.2019.00435.

[20] F.A. Ceppa, et al., Human gut-microbiota interaction in neurodegenerative disorders and current engineered tools for its modeling, Front. Cell. Infect. Microbiol. 10 (July) (Jul. 2020), https://doi.org/10.3389/fcimb.2020.00297.

[21] H.J. Kim, D. Huh, G. Hamilton, D.E. Ingber, Human gut-on-a-chip inhabited by microbial flora that experiences intestinal peristalsis-like motions and flow, Lab Chip 12 (12) (2012) 2165–2174, https://doi.org/10.1039/c2lc40074j.

[22] H. Jung, H. Li, J.J. Collins, D.E. Ingber, Contributions of Microbiome and Mechanical Deformation to Intestinal Bacterial Overgrowth and Inflammation in a Human Gut-On-A-Chip, vol. 13, 2015, https://doi.org/10.1073/pnas.1522193112.

[23] S. Jalili-Firoozinezhad, et al., A complex human gut microbiome cultured in an anaerobic intestine-on-a-chip, Nat. Biomed. Eng. 3 (July) (2019), https://doi.org/10.1038/s41551-019-0397-0.

[24] M.T. Raimondi, D. Albani, C. Giordano, An organ-on-A-chip engineered platform to study the microbiota–gut–brain Axis in neurodegeneration, Trends Mol. Med. 25 (9) (Sep. 2019) 737–740, https://doi.org/10.1016/j.molmed.2019.07.006.

[25] M. Carabotti, A. Scirocco, M.A. Maselli, C. Severi, The gut-brain axis: interactions between enteric microbiota, central and enteric nervous systems, Ann. Gastroenterol. 28 (2) (2015) 203–209.

[26] K. Rea, T.G. Dinan, J.F. Cryan, The microbiome: a key regulator of stress and neuroinflammation, Neurobiology of Stress 4 (Oct. 2016) 23–33, https://doi.org/10.1016/j.ynstr.2016.03.001. Elsevier Inc.

[27] G.A.W. Rook, C.L. Raison, C.A. Lowry, Microbiota, immunoregulatory old friends and psychiatric disorders, Adv. Exp. Med. Biol. 817 (2014) 319–356, https://doi.org/10.1007/978-1-4939-0897-4_15.

[28] T.G. Dinan, J.F. Cryan, Gut instincts: microbiota as a key regulator of brain development, ageing and neurodegeneration, J. Physiol. 595 (2) (Jan. 2017) 489–503, https://doi.org/10.1113/JP273106.

[29] I. Raimondi, L. Izzo, M. Tunesi, M. Comar, D. Albani, C. Giordano, Organ-on-A-chip in vitro models of the brain and the blood-brain barrier and their value to study the microbiota-gut-brain Axis in neurodegeneration, Front. Bioeng. Biotechnol. 7 (January) (2020), https://doi.org/10.3389/fbioe.2019.00435.

[30] T.G. Dinan, J.F. Cryan, Brain-gut-microbiota Axis and mental health, Psychosom. Med. 79 (8) (Oct. 2017) 920–926, https://doi.org/10.1097/PSY.0000000000000519. Lippincott Williams and Wilkins.

[31] K.M. Neufeld, N. Kang, J. Bienenstock, J.A. Foster, Reduced anxiety-like behavior and central neurochemical change in germ-free mice, Neuro Gastroenterol. Motil. 23 (3) (Mar. 2011), https://doi.org/10.1111/j.1365-2982.2010.01620.x.

[32] R.D. Heijtz, et al., Normal gut microbiota modulates brain development and behavior, Proc. Natl. Acad. Sci. U. S. A. 108 (7) (Feb. 2011) 3047–3052, https://doi.org/10.1073/pnas.1010529108.

[33] Y.P. Silva, A. Bernardi, R.L. Frozza, The role of short-chain fatty acids from gut microbiota in gut-brain communication, Front. Endocrinol. 11 (Jan. 2020), https://doi.org/10.3389/fendo.2020.00025. Frontiers Media S.A.

[34] L. Michel, A. Prat, One more role for the gut: microbiota and blood brain barrier, Ann. Transl. Med. 4 (1) (Jan. 2016), https://doi.org/10.3978/j.issn.2305-5839.2015.10.16. AME Publishing Company.

[35] V. Braniste, et al., The gut microbiota influences blood-brain barrier permeability in mice, Sci. Transl. Med. 6 (263) (Nov. 2014), https://doi.org/10.1126/scitranslmed.3009759.

[36] T.C. Fung, C.A. Olson, E.Y. Hsiao, Interactions between the microbiota, immune and nervous systems in health and disease, Nat. Neurosci. 20 (2) (Feb. 2017) 145–155, https://doi.org/10.1038/nn.4476. Nature Publishing Group.

[37] B.B. Williams, et al., Discovery and characterization of gut microbiota decarboxylases that can produce the neurotransmitter tryptamine, Cell Host Microbe 16 (4) (Oct. 2014) 495–503, https://doi.org/10.1016/j.chom.2014.09.001.

[38] R.A. Yunes, et al., GABA production and structure of gadB/gadC genes in Lactobacillus and Bifidobacterium strains from human microbiota, Anaerobe 42 (Dec. 2016) 197–204, https://doi.org/10.1016/j.anaerobe.2016.10.011.

[39] S. Guo, M. Nighot, R. Al-Sadi, T. Alhmoud, P. Nighot, T.Y. Ma, Lipopolysaccharide regulation of intestinal tight junction permeability is mediated by TLR4 signal transduction pathway activation of FAK and MyD88, J. Immunol. 195 (10) (Nov. 2015) 4999–5010, https://doi.org/10.4049/jimmunol.1402598.

[40] R. Zhang, et al., Circulating endotoxin and systemic immune activation in sporadic amyotrophic lateral sclerosis (sALS), J. Neuroimmunol. 206 (1–2) (Jan. 2009) 121–124, https://doi.org/10.1016/j.jneuroim.2008.09.017.

[41] X. Zhan, Gram-negative bacterial molecules associate with Alzheimer disease pathology, Neurology 88 (24) (Jun. 2017) 2338.2–232338, https://doi.org/10.1212/WNL.0000000000004048.

[42] G.C. Brown, The endotoxin hypothesis of neurodegeneration, J. Neuroinflammation 16 (1) (Dec. 2019) 180, https://doi.org/10.1186/s12974-019-1564-7.

[43] J.W. Lee, et al., Neuro-inflammation induced by lipopolysaccharide causes cognitive impairment through enhancement of beta-amyloid generation, J. Neuroinflammation 5 (2008) 1–14, https://doi.org/10.1186/1742-2094-5-37.

[44] M.R. Minter, et al., Antibiotic-induced perturbations in gut microbial diversity influences neuro-inflammation and amyloidosis in a murine model of Alzheimer's disease, Sci. Rep. 6 (May) (2016) 1–12, https://doi.org/10.1038/srep30028.

[45] R. Caesar, V. Tremaroli, P. Kovatcheva-Datchary, P.D. Cani, F. Bäckhed, Crosstalk between gut microbiota and dietary lipids aggravates WAT inflammation through TLR signaling, Cell Metabol. 22 (4) (2015) 658–668, https://doi.org/10.1016/j.cmet.2015.07.026.

[46] Y. He, N. Taylor, X. Yao, A. Bhattacharya, Mouse primary microglia respond differently to LPS and poly(I:C) in vitro, Sci. Rep. 11 (1) (Dec. 2021), 10447, https://doi.org/10.1038/s41598-021-89777-1.

[47] E. d'Hennezel, S. Abubucker, L.O. Murphy, T.W. Cullen, Total lipopolysaccharide from the human gut microbiome silences toll-like receptor signaling, mSystems 2 (6) (2017), https://doi.org/10.1128/msystems.00046-17.

[48] S. Guo, R. Al-Sadi, H.M. Said, T.Y. Ma, Lipopolysaccharide causes an increase in intestinal tight junction permeability in vitro and in vivo by inducing enterocyte membrane expression and localization of TLR-4 and CD14, Am. J. Pathol. 182 (2) (2013) 375–387, https://doi.org/10.1016/j.ajpath.2012.10.014.

[49] R. Okumura, K. Takeda, Maintenance of intestinal homeostasis by mucosal barriers, Inflamm. Regen. 38 (1) (2018) 5, https://doi.org/10.1186/s41232-018-0063-z.

[50] C.T. Capaldo, D.N. Powell, D. Kalman, Layered Defense: How Mucus and Tight Junctions Seal the Intestinal Barrier, 2017, https://doi.org/10.1007/s00109-017-1557-x.

[51] S.S. Ghosh, J. Wang, P.J. Yannie, S. Ghosh, Intestinal barrier dysfunction, LPS translocation, and disease development, J Endocr Soc 4 (2) (Feb. 2020) 1–15, https://doi.org/10.1210/jendso/bvz039.

[52] P. Paone, P.D. Cani, Mucus barrier, mucins and gut microbiota: the expected slimy partners? Gut 69 (12) (Dec. 2020) 2232–2243, https://doi.org/10.1136/gutjnl-2020-322260.

[53] M.E.V. Johansson, et al., The inner of the two Muc2 mucin-dependent mucus layers in colon is devoid of bacteria, Proc. Natl. Acad. Sci. U.S.A. 105 (39) (2008) 15064–15069, https://doi.org/10.1073/pnas.0803124105.

[54] A.N. Round, N.M. Rigby, A. Garcia de la Torre, A. Macierzanka, E.N.C. Mills, A. R. Mackie, Lamellar structures of MUC2-rich mucin: a potential role in governing the barrier and lubricating functions of intestinal mucus, Biomacromolecules 13 (10) (2012) 3253–3261, https://doi.org/10.1021/bm301024x.

[55] A. Macierzanka, A.R. Mackie, B.H. Bajka, N.M. Rigby, F. Nau, D. Dupont, Transport of particles in intestinal mucus under simulated infant and adult physiological conditions: impact of mucus structure and extracellular DNA, PLoS One 9 (4) (2014) 1–11, https://doi.org/10.1371/journal.pone.0095274.

[56] L. Sardelli, et al., ' towards bioinspired in vitro models of intestinal mucus ', RSC Adv. 9 (28) (2019) 15887–15899, https://doi.org/10.1039/c9ra02368b.

[57] M. Boegh, S.G. Baldursdóttir, A. Müllertz, H.M. Nielsen, Property profiling of biosimilar mucus in a novel mucus-containing in vitro model for assessment of intestinal drug absorption, Eur. J. Pharm. Biopharm. 87 (2) (2014) 227–235, https://doi.org/10.1016/j.ejpb.2014.01.001.

[58] D. Peneda Pacheco, N. Suárez Vargas, S. Visentin, P. Petrini, From tissue engineering to engineering tissues: the role and application of in vitro models, Biomater. Sci. (2020), https://doi.org/10.1039/D0BM01097A.

[59] L. Liu, et al., Models to evaluate the barrier properties of mucus during drug diffusion, Int. J. Pharm. 599 (1) (2021), 120415, https://doi.org/10.1016/j.ijpharm.2021.120415.

[60] D.P. Pacheco, et al., Disassembling the complexity of mucus barriers to develop a fast screening tool for early drug discovery, J. Mater. Chem. B (2019), https://doi.org/10.1039/c9tb00957d.

[61] C. Butnarasu, G. Caron, D.P. Pacheco, P. Petrini, S. Visentin, Cystic fibrosis mucus model to design more efficient drug therapies, Mol. Pharm. (Dec. 2021), 1c00644, https://doi.org/10.1021/acs.molpharmaceut.1c00644 acs.molpharmaceut.

[62] M.A. Signore, C. De Pascali, L. Giampetruzzi, P.A. Siciliano, L. Francioso, Gut-on-Chip microphysiological systems: latest advances in the integration of sensing strategies and adoption of mature detection mechanisms, Sens Biosensing Res 33 (Aug. 2021), 100443, https://doi.org/10.1016/j.sbsr.2021.100443.

[63] W. Shin, H.J. Kim, Intestinal barrier dysfunction orchestrates the onset of inflammatory host-microbiome cross-talk in a human gut inflammation-on-a-chip, Proc. Natl. Acad. Sci. U. S. A. 115 (45) (2018) E10539–E10547, https://doi.org/10.1073/pnas.1810819115.

[64] Z. Jia, Z. Guo, C.-T. Yang, C. Prestidge, B. Thierry, "Mucus-on-Chip": a new tool to study the dynamic penetration of nanoparticulate drug carriers into mucus, Int. J. Pharm. 598 (January) (Apr. 2021), 120391, https://doi.org/10.1016/j.ijpharm.2021.120391.

[65] J.P. Nataro, J.B. Kaper, Diarrheagenic *Escherichia coli*, Clin. Microbiol. Rev. 11 (2) (Apr. 1998) 403, https://doi.org/10.1128/CMR.11.2.403, 403.

[66] E. Voss, A.W. Paton, P.A. Manning, J.C. Paton, Molecular analysis of shiga toxigenic *Escherichia coli* O111:H $^{-}$ proteins which react with sera from patients with hemolytic-uremic syndrome, Infect. Immun. 66 (4) (Apr. 1998) 1467–1472, https://doi.org/10.1128/IAI.66.4.1467-1472.1998.

[67] A. Vojdani, E. Vojdani, E. Saidara, D. Kharrazian, Reaction of amyloid-β peptide antibody with different infectious agents involved in alzheimer's disease, J. Alzheim. Dis. 63 (2) (Apr. 2018) 847–860, https://doi.org/10.3233/JAD-170961.

[68] M. Kuroda, et al., Serum tau protein as a marker of disease activity in enterohemorrhagic Escherichia coli O111-induced hemolytic uremic syndrome, Neurochem. Int. 85 (86) (Jun. 2015) 24–30, https://doi.org/10.1016/j.neuint.2015.04.003.

[69] M.A. Spivey, S.L. Dunn-Horrocks, T. Duong, Epithelial cell adhesion and gastrointestinal colonization of Lactobacillus in poultry, Poultry Sci. 93 (11) (Nov. 2014) 2910–2919, https://doi.org/10.3382/ps.2014-04076.

[70] H. Embaye, R.M. Batt, J.R. Saunders, B. Getty, C.A. Hart, Interaction of enteropathogenic Escherichia coli 0111 with rabbit intestinal mucosa in vitro, Gastroenterology 96 (4) (Apr. 1989) 1079–1086, https://doi.org/10.1016/0016-5085(89)91626-0.

[71] F.A. Miller, A. Sacco, A.L. David, A.K. Boyle, Interventions for infection and inflammation-induced preterm birth: a preclinical systematic review, Reprod. Sci. 30 (2) (Feb. 2023) 361–379, https://doi.org/10.1007/s43032-022-00934-x.

[72] L. Sun, et al., Myeloid-specific gene deletion of protein phosphatase 2A magnifies MyD88- and TRIF-dependent inflammation following endotoxin challenge, J. Immunol. 198 (1) (Jan. 2017) 404–416, https://doi.org/10.4049/jimmunol.1600221.

[73] W. Shin, H.J. Kim, Pathomimetic Modeling of Human Intestinal Diseases and Underlying Host-Gut Microbiome Interactions in a Gut-On-A-Chip, 2018, pp. 135–148, https://doi.org/10.1016/bs.mcb.2018.05.006.

[74] H.J. Kim, H. Li, J.J. Collins, D.E. Ingber, Contributions of microbiome and mechanical deformation to intestinal bacterial overgrowth and inflammation in a human gut-on-a-chip, Proc. Natl. Acad. Sci. USA 113 (1) (Jan. 2016), https://doi.org/10.1073/pnas.1522193112.

[75] L. Sardelli, et al., Bioinspired in vitro intestinal mucus model for 3D-dynamic culture of bacteria, Biomater. Adv. 139 (Aug. 2022), 213022, https://doi.org/10.1016/J.BIOADV.2022.213022.

[76] P. Matricardi, F. Alhaique, T. Coviello, Polysaccharide Hydrogels, 2016.

[77] G. Guagliano, et al., 'Hep3Gel: A Shape-Shifting Extracellular Matrix-Based, Three-Dimensional Liver Model Adaptable to Different Culture Systems', 2022, https://doi.org/10.1021/acsbiomaterials.2c01226.

[78] B.T. Stokke, 'Polysaccharide hydrogels', Gels 5 (3) (Jul. 29, 2019) 38, https://doi.org/10.3390/gels5030038.

[79] J. Beal, et al., Robust estimation of bacterial cell count from optical density, Commun. Biol. 3 (1) (Sep. 2020) 1–29, https://doi.org/10.1038/s42003-020-01127-5, 2020 3:1.

[80] F. Donnaloja, et al., Human gut epithelium features recapitulated in MINERVA 2.0 millifluidic organ-on-a-chip device, APL Bioeng. 7 (3) (Sep. 2023), 36117, https://doi.org/10.1063/5.0144862.

[81] C. Giordano, M.T. Raimondi, L. Izzo, M. Laganà, D. Albani, P. Petrini, Millifluidic Device for Advanced Cultures of Biological Agents, Mar. 2022 doi: US202/0340854A1.

[82] F. Fanizza et al., 'Development of an Induced Pluripotent Stem Cell-Based Liver-On-A-Chip Assessed with an Alzheimer's Disease Drug', doi: 10.1021/acsbiomaterials.3c00346.

[83] A. Mulak, B. Bonaz, Brain-gut-microbiota axis in Parkinson's disease, World J. Gastroenterol. 21 (37) (2015) 10609–10620, https://doi.org/10.3748/wjg.v21.i37.10609.

[84] D. Peneda Pacheco, N. Suárez Vargas, S. Visentin, P. Petrini, From tissue engineering to engineering tissues: the role and application of: the vitro models, Biomater. Sci. 9 (1) (2021) 70–83, https://doi.org/10.1039/d0bm01097a.

[85] L. Sardelli, Engineering an Innovative Techno-Logical Tool to Address the Micro-biota Impact on Brain Functionality in a Multiorgan-On-Chip Platform, 2022. Milano.

[86] J. Lee, J.H. Choi, H.J. Kim, Human gut-on-a-chip technology: will this revolutionize our understanding of IBD and future treatments? Expet Rev. Gastroenterol. Hepatol. 10 (8) (2016) 883–885, https://doi.org/10.1080/17474124.2016.1200466.

[87] H.J. Kim, H. Li, J.J. Collins, D.E. Ingber, Contributions of microbiome and mechanical deformation to intestinal bacterial overgrowth and inflammation in a human gut-on-a-chip, Proc. Natl. Acad. Sci. U. S. A. 113 (1) (Jan. 2016) E7–E15, https://doi.org/10.1073/pnas.1522193112.

[88] L. Sardelli, et al., Technological tools and strategies for culturing human gut microbiota in engineered in vitro models, Biotechnol. Bioeng. 118 (8) (Aug. 01, 2021) 2886–2905, https://doi.org/10.1002/bit.27816. John Wiley and Sons Inc.

[89] C.T. Capaldo, D.N. Powell, D. Kalman, Layered defense: how mucus and tight junctions seal the intestinal barrier, J. Mol. Med. 95 (9) (2017) 927–934, https://doi.org/10.1007/s00109-017-1557-x.

[90] I. Leake, Mucus—is it time to change your gut reaction? Nat. Rev. Gastroenterol. Hepatol. 10 (11) (Nov. 2013) 622, https://doi.org/10.1038/nrgastro.2013.200, 622.

[91] L. Boeri, L. Izzo, L. Sardelli, M. Tunesi, D. Albani, C. Giordano, Advanced organ-on-a-chip devices to investigate liver multi-organ communication: Focus on gut, microbiota and brain, Bioengineering 6 (4) (Sep. 2019) 91, https://doi.org/10.3390/bioengineering6040091.

[92] Y. Xiang, H. Wen, Y. Yu, M. Li, X. Fu, S. Huang, Gut-on-chip: recreating human intestine in vitro, J. Tissue Eng. 11 (Jan. 2020), 204173142096531, https://doi.org/10.1177/2041731420965318.

[93] H. Suhaimi, S. Wang, T. Thornton, D.B. Das, On glucose diffusivity of tissue engineering membranes and scaffolds, Chem. Eng. Sci. 126 (2015) 244–256, https://doi.org/10.1016/j.ces.2014.12.029.

[94] F. Qu, et al., Maturation state and matrix microstructure regulate interstitial cell migration in dense connective tissues, Sci. Rep. 8 (1) (2018) 1–13, https://doi.org/10.1038/s41598-018-21212-4.

[95] M. Merli, et al., Pectin-based bioinks for 3D models of neural tissue produced by a pH-controlled kinetics, Front. Bioeng. Biotechnol. 10 (Dec. 2022) 2362, https://doi.org/10.3389/FBIOE.2022.1032542/BIBTEX.

[96] C.M. Silva, A.J. Ribeiro, I.V. Figueiredo, A.R. Gonçalves, F. Veiga, Alginate microspheres prepared by internal gelation: development and effect on insulin stability, Int. J. Pharm. 311 (1–2) (2006) 1–10, https://doi.org/10.1016/j.ijpharm.2005.10.050.

[97] X.D. Liu, et al., Characterization of structure and diffusion behaviour of Ca-alginate beads prepared with external or internal calcium sources, J. Microencapsul. 19 (6) (Jan. 2002) 775–782, https://doi.org/10.1080/02652040210000022743.

[98] D.N.P. Murthy, M. Bulmer, J.A. Eccleston, Weibull model selection for reliability modelling, Reliab. Eng. Syst. Saf. 86 (3) (2004) 257–267, https://doi.org/10.1016/j.ress.2004.01.014.

[99] V. Papadopoulou, K. Kosmidis, M. Vlachou, P. Macheras, On the use of the Weibull function for the discernment of drug release mechanisms, Int. J. Pharm. 309 (1–2) (2006) 44–50, https://doi.org/10.1016/j.ijpharm.2005.10.044.

[100] J. Miao, M. Tsige, P.L. Taylor, Generalized model for the diffusion of solvents in glassy polymers: from Fickian to Super Case II, J. Chem. Phys. 147 (4) (2017) 1–15, https://doi.org/10.1063/1.4994924.

[101] D.F. Stamatialis, M. Sanopoulou, J.H. Petropoulos, Investigation of case II diffusion behavior. 2. Study of the poly(methyl methacrylate)-methyl alcohol system by two-beam microinterferometry, Macromolecules 35 (3) (2002) 1021–1027, https://doi.org/10.1021/ma001409b.

[102] P.E. Shaw, P.L. Burn, Real-time fluorescence quenching-based detection of nitro-containing explosive vapours: what are the key processes? Phys. Chem. Chem. Phys. 19 (44) (2017) 29714–29730, https://doi.org/10.1039/C7CP04602B.

[103] A. Macierzanka, A.R. Mackie, L. Krupa, Permeability of the small intestinal mucus for physiologically relevant studies: impact of mucus location and ex vivo treatment, Sci. Rep. 9 (1) (2019) 1–12, https://doi.org/10.1038/s41598-019-53933-5.

[104] L. Zheng, C.J. Kelly, S.P. Colgan, Physiologic hypoxia and oxygen homeostasis in the healthy intestine. A review in the theme: cellular responses to hypoxia, Am. J. Physiol. Cell Physiol. 309 (6) (Sep. 2015) C350–C360, https://doi.org/10.1152/ajpcell.00191.2015.

[105] A. Flannery, J. Gerlach, L. Joshi, M. Kilcoyne, Assessing bacterial interactions using carbohydrate-based microarrays, Microarrays 4 (4) (2015) 690–713, https://doi.org/10.3390/microarrays4040690.

[106] G.M. Hirschfield, J. Herbert, M.C. Kahan, M.B. Pepys, Human C-reactive protein does not protect against acute lipopolysaccharide challenge in mice, J. Immunol. 171 (11) (2003) 6046–6051, https://doi.org/10.4049/jimmunol.171.11.6046.

[107] C.D. Ciornei, et al., Biofilm-forming Pseudomonas aeruginosa Bacteria Undergo Lipopolysaccharide Structural Modifications and Induce Enhanced Inflammatory Cytokine Response in Human Monocytes, vol. 5, 2010, pp. 288–301, https://doi.org/10.1177/1753425909341807.

[108] M.M. Vroom, Y. Rodriguez-Ocasio, J.B. Lynch, E.G. Ruby, J.S. Foster, Modeled microgravity alters lipopolysaccharide and outer membrane vesicle production of

the beneficial symbiont Vibrio fischeri, npj Microgravity 7 (1) (Mar. 2021) 1–10, https://doi.org/10.1038/s41526-021-00138-8, 2021 7:1.
[109] J. Zur, D. Wojcieszyńska, U. Guzik, Metabolic responses of bacterial cells to immobilization, Molecules 21 (7) (2016), https://doi.org/10.3390/molecules21070958.
[110] E.P. Da Silva, et al., Drug release profile and reduction in the in vitro burst release from pectin/HEMA hydrogel nanocomposites crosslinked with titania, RSC Adv. 6 (23) (2016) 19060–19068, https://doi.org/10.1039/c5ra27865a.
[111] E. Ning, et al., 3D bioprinting of mature bacterial biofilms for antimicrobial resistance drug testing, Biofabrication 11 (4) (2019), https://doi.org/10.1088/1758-5090/ab37a0.
[112] M.G. Wiebe, K. Koivuranta, M. Penttilä, L. Ruohonen, Lipid production in batch and fed-batch cultures of Rhodosporidium toruloides from 5 and 6 carbon carbohydrates, BMC Biotechnol. 12 (May 2014) (2012), https://doi.org/10.1186/1472-6750-12-26.
[113] L. dos Reis, et al., Increased production of cellulases and xylanases by Penicillium echinulatum S1M29 in batch and fed-batch culture, Bioresour. Technol. 146 (2013) 597–603, https://doi.org/10.1016/j.biortech.2013.07.124.
[114] Y.H. Cho, et al., Production of nattokinase by batch and fed-batch culture of Bacillus subtilis, N. Biotech. 27 (4) (2010) 341–346, https://doi.org/10.1016/j.nbt.2010.06.003.
[115] B. Tilocca, et al., Gut–brain axis and neurodegeneration: state-of-the-art of meta-omics sciences for microbiota characterization, Int. J. Mol. Sci. 21 (11) (2020) 1–20, https://doi.org/10.3390/ijms21114045.
[116] W. Shin, et al., A robust longitudinal co-culture of obligate anaerobic gut microbiome with human intestinal epithelium in an anoxic-oxic interface-on-a-chip, Front. Bioeng. Biotechnol. 7 (FEB) (2019), https://doi.org/10.3389/fbioe.2019.00013.
[117] R. Blechová, D. Pivodová, Limulus amoebocyte lysate (LAL) test - an alternative method for detection of bacterial endotoxins, Acta Vet. 70 (3) (2001) 291–296, https://doi.org/10.2754/avb200170030291.
[118] H.J. Kim, D. Huh, G. Hamilton, D.E. Ingber, Human gut-on-a-chip inhabited by microbial flora that experiences intestinal peristalsis-like motions and flow, Lab Chip 12 (12) (2012) 2165, https://doi.org/10.1039/c2lc40074j.
[119] C. Butnarasu, G. Caron, D.P. Pacheco, P. Petrini, S. Visentin, Cystic fibrosis mucus model to design more efficient drug therapies, Mol. Pharm. (Dec. 2021), 1c00644, https://doi.org/10.1021/acs.molpharmaceut.1c00644 acs.molpharmaceut.
[120] M. Oriano, et al., The open challenge of in vitro modeling complex and multi-microbial communities in three-dimensional niches, Front. Bioeng. Biotechnol. 8 (October) (2020) 1–17, https://doi.org/10.3389/fbioe.2020.539319.
[121] A.F. de Vos, J.M. Pater, P.S. van den Pangaart, M.D. de Kruif, C. van 't Veer, T. van der Poll, In vivo lipopolysaccharide exposure of human blood leukocytes induces cross-tolerance to multiple TLR ligands, J. Immunol. 183 (1) (2009) 533–542, https://doi.org/10.4049/jimmunol.0802189.
[122] H. Shi, et al., The in vitro effect of lipopolysaccharide on proliferation, inflammatory factors and antioxidant enzyme activity in bovine mammary epithelial cells, Animal Nutrition 2 (2) (2016) 99–104, https://doi.org/10.1016/j.aninu.2016.03.005.
[123] T.C. Savidge, et al., Lipopolysaccharide-induced human enterocyte tolerance to cytokine-mediated interleukin-8 production may occur independently of TLR-4/MD-2 signaling, Pediatr. Res. 59 (1) (2006) 89–95, https://doi.org/10.1203/01.pdr.0000195101.74184.e3.
[124] W. Fang, et al., Effects of Qing Hua Chang Yin on lipopolysaccharide-induced intestinal epithelial tight junction injury in Caco-2 cells, Mol. Med. Rep. 23 (3) (Mar. 2021) 1, https://doi.org/10.3892/MMR.2021.11844/HTML, 1.
[125] S. He, Y. Guo, J. Zhao, X. Xu, N. Wang, Q. Liu, Ferulic acid ameliorates lipopolysaccharide-induced barrier dysfunction via MicroRNA-200c-3p-mediated activation of PI3K/AKT pathway in caco-2 cells, Front. Pharmacol. 11 (Apr. 2020), 509267, https://doi.org/10.3389/FPHAR.2020.00376/BIBTEX.
[126] G. Trujillo-de Santiago, M.J. Lobo-Zegers, S.L. Montes-Fonseca, Y.S. Zhang, M. M. Alvarez, Gut-microbiota-on-a-chip: an enabling field for physiological research, Microphysiol Syst 1 (3) (2018) 1, https://doi.org/10.21037/mps.2018.09.01, 1.